JGR Solid Earth

RESEARCH ARTICLE
10.1029/2024JB030689

A Decadal Survey of the Near-Surface Seismic Velocity Response to Hydrological Variations in Utah, United States

Kuan-Fu Feng[1,2], Marine Denolle[1], Fan-Chi Lin[2], and Tonie van Dam[2]

[1]Department of Earth and Space Sciences, University of Washington, Seattle, WA, USA, [2]Department of Geology and Geophysics, University of Utah, Salt Lake City, UT, USA

Key Points:

- Multi-year wet-dry water cycles are closely consistent with dv/v observations, notably at stations within the Great Salt Lake watershed
- The annual dv/v variations and their peak times closely correspond to expected water cycle patterns in Utah
- Using long-term lake level as a groundwater proxy in modeling reveals regional recharge timing differences driven by elevation and snowmelt

Supporting Information:

Supporting Information may be found in the online version of this article.

Correspondence to:

K.-F. Feng,
kuanfu.feng@utah.edu

Citation:

Feng, K.-F., Denolle, M., Lin, F.-C., & van Dam, T. (2026). A decadal survey of the near-surface seismic velocity response to hydrological variations in Utah, United States. *Journal of Geophysical Research: Solid Earth*, *131*, e2024JB030689. https://doi.org/10.1029/2024JB030689

Received 2 NOV 2024
Accepted 2 JAN 2026

Author Contributions:

Conceptualization: Kuan-Fu Feng, Marine Denolle, Fan-Chi Lin
Data curation: Kuan-Fu Feng, Tonie van Dam
Formal analysis: Kuan-Fu Feng
Funding acquisition: Marine Denolle, Fan-Chi Lin
Investigation: Kuan-Fu Feng, Marine Denolle
Methodology: Kuan-Fu Feng, Marine Denolle
Project administration: Marine Denolle, Fan-Chi Lin
Resources: Marine Denolle, Fan-Chi Lin
Software: Kuan-Fu Feng
Supervision: Marine Denolle, Fan-Chi Lin
Validation: Kuan-Fu Feng

Abstract Ongoing climate change is leading to an increase in prolonged droughts and severe weather events, which are particularly pronounced in semi-arid regions, such as the western United States. These extremes could have lasting social and environmental impacts. Continuous monitoring of near-surface hydrological processes and groundwater resources provides helpful information for effective water resource management. The seismological signature of groundwater fluctuations is clear in the temporal variations in seismic velocities, dv/v. To this end, developing a proxy for groundwater level using dv/v represents an opportunity, but further understanding of the relation between dv/v and subsurface hydrology is required. In this study, we apply single-station cross-component correlation analysis to 28 broadband seismic stations in Utah between January 2006 and March 2023 and analyze the dv/v in the 2–4 Hz frequency band. To explain dv/v, we linearly superimpose thermoelastic stresses, soil moisture estimated from remote sensing data products, and a long-term deep water table pore pressure. We find that the relative contributions of each depend on the location. Still, adding a long-term water table decline, which is not systematically observed in soil moisture, better fits our data. We conclude that soil moisture alone does not explain the variations in total water storage when subsurface moisture is decoupled from the deep-water table. We also conclude that dv/v can be used as a proxy for water storage.

Plain Language Summary Climate change makes droughts and water shortages more common in the western United States. Tracking how water moves and is stored underground is essential for understanding these changes, but traditional tools such as monitoring wells and satellites cover too little ground or lack enough detail. In this study, we used small changes in the speed of seismic waves, "dv/v," recorded at 28 seismic stations across Utah over more than a decade. These subtle changes help reveal how water flows and accumulates below the surface. By combining dv/v data with estimates of soil moisture and long-term lake level changes (used as a proxy for groundwater), we built a model to separate the effects of shallow and deep-water processes. We found that dv/v can detect seasonal and long-term shifts in subsurface water, and deep groundwater changes are significant in some areas. This seismic method offers a powerful new way to monitor underground water across large regions, bridging the gap between scattered well data and coarse satellite data. Our approach may help scientists and water managers better understand and adapt to changing water availability in a warming climate.

1. Introduction

Due to ongoing climate change, widespread droughts and extreme weather events have become more common in recent years (Coumou & Rahmstorf, 2012; Hulme, 2014). The increasing frequency and severity of droughts could lead to enduring impacts on society and the environment (Khatri & Strong, 2020; Schwabe et al., 2013). Utah is situated in a semi-arid region of the western US, characterized by limited water availability. Water resource management is crucial for the state. The water supply in Utah relies on the snowpack that accumulates in the winter, and groundwater and stream flow control the runoff during the dry season (Brooks et al., 2021; Utah State Water Resource Plan, 2021). There are several lakes and reservoirs across the state that capture snowmelt runoff. The Great Salt Lake (GSL) is the largest endorheic lake in North America and serves as the terminus for various rivers, streams, and subsurface groundwater within its extensive catchment area. Due to its salinity, GSL does not directly contribute to the regional water supply, but its water level has been considered one of the primary indicators of the state of regional water resources. The GSL has experienced periods of extended drought throughout its history, including years of shortages and years of replenishment (Wang et al., 2012; Utah Division of Water Resources, https://water.utah.gov/great-salt-lake/, last accessed 01/2023). Nowadays, the GSL is facing the challenges of declining water levels, which have lowered by more than 3 m since 1999 (Hassan et al., 2023).

Visualization: Kuan-Fu Feng
Writing – original draft: Kuan-Fu Feng
Writing – review & editing: Kuan-Fu Feng, Marine Denolle, Fan-Chi Lin, Tonie van Dam

Prolonged droughts can severely impact the lake's ecosystem and overall health (Baxter & Butler, 2020; Null & Wurtsbaugh, 2020). However, the uncertainty associated with the groundwater inflow makes it difficult to accurately assess the GSL water budget.

Conventionally, monitoring groundwater levels, whether in aquifers or as subsurface moisture, requires in situ instrumentation (i.e., wells and probes) with site-specific sensitivities. These measurements represent the site's ground truth for water storage but have two limitations. First, data collection from ground-based sensors, that is, wells and probes, has historically been varied. Second, although recent efforts (e.g., Perrone & Jasechko, 2017) have expanded access to well data, the information remains fragmented across numerous databases with varying standards, limiting its broader utility. Alternatively, remote sensing techniques provide increasingly frequent measurements (~3 days) and a low spatial resolution (~10–35 km) (e.g., Tangdamrongsub et al., 2020). Temporal water mass variation on a much larger scale can be monitored using remote sensing (e.g., GRACE; Landerer & Swenson, 2012) despite the relatively low spatial resolution at around a few hundred kilometers. Ford and Quiring (2019) comprehensively compared soil moisture measurements for subsurface moisture, especially in situ with modeled products and remote-sensing-based derived estimates. They concluded that both the North American Land Data Assimilation System project phase 2 (NLDAS-2) and the Soil Moisture Active Passive (SMAP) consistently performed best. Improved parameterization, models, or proxies of near-surface water remain a desirable avenue of research.

The seismology community has recently demonstrated the potential of linking seismic velocity changes (dv/v) with hydrological variations, where intermediate spatial sensitivity and resolution from a few meters to kilometers can be achieved. The time resolution ranges from hours to decades, depending on the station operation period and research purpose. Many studies have reported a strong (anti-)correlation (e.g., instantaneous response) between perturbation in seismic velocities and subsurface hydrological variables such as groundwater level changes and soil moisture variations (Clements & Denolle, 2018; Gassenmeier et al., 2014; Illien et al., 2021; Lecocq et al., 2017; Mao et al., 2022, 2025; Oakley et al., 2021; Sens-Schönfelder & Wegler, 2006; Shen et al., 2024; Vittecoq et al., 2025; Voisin et al., 2016). Because the method relies solely on passive seismic noise and can utilize existing seismic stations, it offers a flexible and logistically favorable way to monitor subsurface hydrological parameters at the mesoscale. This method, known as time-lapse passive seismic interferometry, measures coda wave perturbations from repeating waveforms and infers dv/v. The repeated waveform can be obtained from either repeated sources or noise correlation functions calculated using different time windows (Pacheco & Snieder, 2005; Sens-Schönfelder & Wegler, 2006; Snieder et al., 2002; Weaver & Lobkis, 2004).

Variations in groundwater levels in the subsurface induce local changes in effective pressure, leading to changes in seismic velocities. In fully saturated media, for example, below the water table, changes in rigidity, the ability of rocks to resist shear stresses, are reduced with increasing pore pressure (e.g., Clements & Denolle, 2023; Fokker et al., 2021; Ostrovsky & Johnson, 2001), which leads to a reduction in shear wave speed. Density changes due to pore pressure changes are not large because of the incompressibility of rocks and water (Fokker et al., 2021). Still, dv/v has been correlated with dilatational strains empirically (Donaldson et al., 2019; Hotovec-Ellis et al., 2022; Sens-Schönfelder & Eulenfeld, 2019; Takano et al., 2019) and as predicted from the earthquake-related drop/healing behaviors or temperature-humidity coupling effects under a non-linear elasticity framework (Clements & Denolle, 2023; Diewald et al., 2024; Hobiger et al., 2014; Okubo et al., 2024). Above the water table, in partially saturated media, both rigidity and density are affected by relative water content, and more complex physics, which depends on pore water distribution, may affect the wave speed (e.g., Illien et al., 2021; Oakley et al., 2021; Shen et al., 2024; Solazzi et al., 2021). Seismic waves have spatial resolution and sensitivity that depend on their wavelengths: high-frequency signals can have relatively high spatial resolution (e.g., 500 m/s shallow seismic waves at 5 Hz have a 100-m wavelength) and shallow depth sensitivity compared to low-frequency signals, considering the surface waves dominant codas (Obermann et al., 2013, 2016; Yuan et al., 2021). Therefore, shear waves are helpful to track groundwater changes at intermediate spatial resolutions (e.g., Delouche & Stehly, 2023; Gaubert-Bastide et al., 2022; Mao et al., 2025). Because seismic signals are continuously recorded, they can be used to monitor, at least at the hourly time scale, water levels at the mesoscale.

One outstanding issue remains on the relative contribution of saturation (or moisture) changes in partially saturated media and pore pressure changes below the water table. Indeed, the depth resolution is relatively smooth in surface waves, and conventional networks of seismometers do not permit precise depth analysis. Illien et al. (2021) were the first to propose a model that combines groundwater storage and subsurface moisture to

explain the surface observations of dv/v. They relied on in situ moisture and geochemical tracer measurements for groundwater depth to discriminate between the two water storages. They found that the intermittent coupling of subsurface water with groundwater during replenishment cycles in Nepal can explain the dv/v observations. Recent advances demonstrate that seismic observations can directly benefit hydrologists by revealing subsurface hydrological dynamics that are difficult to capture using conventional measurements. Sun et al. (2025) use high-resolution distributed acoustic sensing (DAS) to characterize rapid hydro-thermal activities in frozen and partially frozen soils, providing new insights into cryosphere–hydrology interactions and their mechanical signals. Likewise, Shen et al. (2024) employed fiber-optic seismic sensing to resolve detailed vadose-zone soil moisture changes at high spatial resolution. At larger scales, Lesparre et al. (2024) demonstrate that seismic refraction can help image the hydrofacies architecture, substantially enhancing hydrological model parameterization and groundwater flow predictions. These examples show that passive and active seismic methods, especially combined with DAS, electrical, or soil-moisture sensing, give hydrologically continuous, detailed data on infiltration, water-table changes, freeze–thaw, and subsurface hydro-mechanical interactions. While multi-sensor networks and seismic refraction experiments are increasingly valued and deployed (e.g., Lesparre et al., 2024; Oakley et al., 2021; Shen et al., 2024; Sun et al., 2025), they often span only short-term experiments. Here, we tackle the problem of differentiating the relative contributions of saturation in the vadose zone and pore pressure beneath the water table, across a regional scale, using decades of seismic data. Long-term dv/v observations offer a unique perspective on subsurface water dynamics, complementing traditional monitoring measurements with sustained, spatially extensive insights.

This study analyzes continuous seismic recordings from 28 broadband seismic stations across Utah (Figure 1) from January 2006 to March 2023. We highlight the connection between seismic velocity variations and hydrological observations. Utah's hydrology features snowmelt-driven surface water, an arid to semi-arid climate, and complex groundwater systems that respond significantly to climatic and anthropogenic changes. Understanding these processes is essential for explaining this region's temporal variations in subsurface seismic properties. The manuscript is organized as follows: Section 2 introduces the data set and methodology used in this work. We use single-station measurements to determine the temporal evolution of dv/v (e.g., Clements & Denolle, 2023; Feng et al., 2021; Hobiger et al., 2014; etc.). Section 3 presents the seasonality and co-evolutions between the observed dv/v, GSL, Utah Lake water levels, and near-surface moisture. Assuming linear superposition, we investigate the relationship between dv/v variations and the potential hydrological signatures. Section 4 discusses the regional pattern of the observed dv/v and the dominant factors influencing it. Finally, this study highlights the value of time-lapse passive seismic interferometry in monitoring and understanding hydrological processes in semi-arid regions. Such insights are essential for developing sustainable resource management strategies that benefit both society and the environment in the context of climate change.

2. Data and Methodologies

2.1. Hydrological Data

2.1.1. The Great Salt Lake (GSL) and Utah Lake

The GSL (Figure 1), the largest terminal lake in North America, is the remnant of the larger Pleistocene Lake Bonneville. It is an essential natural and economic resource for the region. On the other hand, Utah Lake (Figure 1), located south of the GSL, is a freshwater lake fed by several rivers, with the Jordan River as its outlet, flowing northward into the GSL. We gather GSL water level data from the United States Geological Survey (USGS) Water Resources (https://dashboard.waterdata.usgs.gov, last accessed 10/2022, Site No. 10010100). It shows roughly an annual water level variation of ∼1.2 m (∼4 ft) on top of a long-term dry-wet cycle of nearly 3 m (Figure 2a). The Utah Lake water level is estimated from the storage volume obtained from the Snowpack Telemetry (SNOTEL) Utah reservoir site (Site No. 10166500), operated by the Natural Resources Conservation Service (NRCS) of the United States Department of Agriculture (USDA, https://www.nrcs.usda.gov/, last accessed 04/2023). We estimate the water level by dividing the storage volume by the lake area of 384.4513 km^2 (95,000 Acres). Its water level exhibits long-term dry-wet variations (Figure 2b), similar to the GSL. Its annual variation is ∼1 m.

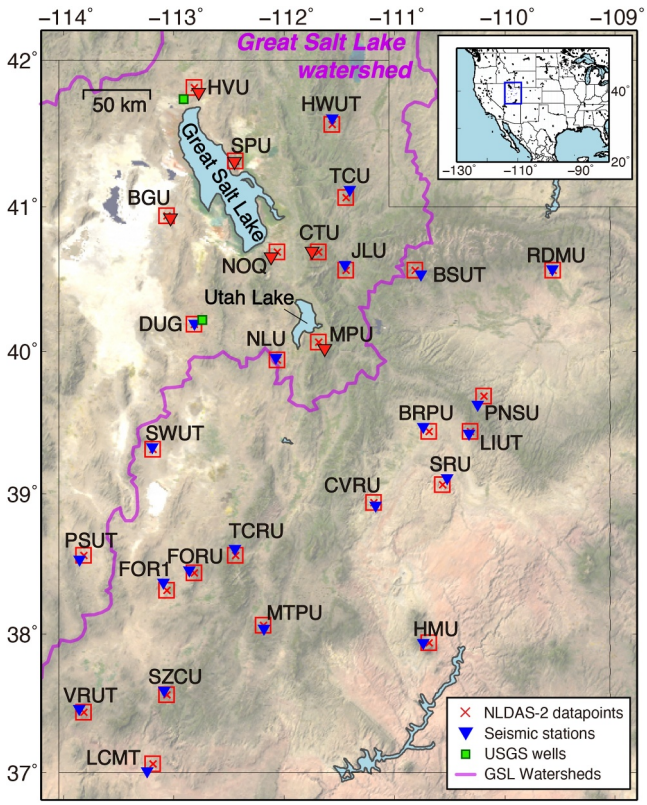

Figure 1. Station map. The inverted triangles represent the broadband seismic stations used in this study. The red inverted triangles identify the stations whose time series are shown in Figure 4. The green squares are the two closest groundwater wells used for comparison. Red crosses are the soil moisture equivalent water thickness (SM-EWT) data points from the NLDAS-2 model. The square encircles the area of the selected grid unit (0.125° × 0.125°) of the center of the "x." The area surrounded by the pink line encompasses the Great Salt Lake watershed (from the Utah Division of Water Resources, https://water.utah.gov/).

2.1.2. Soil Moisture Equivalent Water Thickness (SM-EWT)

Moisture in vadose (unsaturated) zones also plays a crucial role in the near-surface water resources (Illien et al., 2021; Shen et al., 2024). However, due to the lack of co-located hydrological measurements, we characterized soil moisture equivalent water thickness (SM-EWT) using North American Land Data Assimilation System (NLDAS-2) (Xia, Mitchell, Ek, Cosgrove, et al., 2012; Xia, Mitchell, Ek, Sheffield, et al., 2012) as the near-surface water content for comparison. NLDAS was developed by a nationwide multi-institution partnership (Mitchell et al., 2004). NLDAS ingests various observational data, such as satellite remote sensing measurements, ground-based weather station data, and radar-based rainfall estimates. These data are assimilated into sophisticated land surface models (LSMs) to produce gridded outputs (0.125° × 0.125° ≅ 14 km × 14 km), including terms related to surface energy and water budgets. To compare SM-EWT to our dv/v observations, we extract the SM-EWT data from the closest grid point to the seismic stations (see Figure 1). The locations are usually within ~9.3 km. The average annual variations of SM-EWT range from 0.05 to 0.22 m. Figure 2c shows an SM-EWT time series as an example at Station CVRU.

2.1.3. Jordanelle Reservoir

The Jordanelle Reservoir is located approximately 3 km from seismic station JLU. The reservoir serves multiple purposes, including water storage, flood control, and recreation. Therefore, its highest and lowest water levels differ from those of other surface water bodies (the blue curve in Figure 2d). We collected the reservoir's monthly water levels from the United States Bureau of Reclamation (https://data.usbr.gov, last accessed 04/2023). Station JLU is located on a mountain crest. While the hydraulic connectivity of this site to the reservoir is unclear, considering its proximity, its subsurface velocity variations could be affected by the reservoir's poroelastic loading in response to the 30-m annual water level variations.

2.1.4. Groundwater Wells

For in situ groundwater data, in our study area, most wells are in the valley and exhibit irregular time resolution for data collection. However, two wells managed by the USGS Utah Water Science Center (https://www.usgs.gov/centers/utah-water-science-center, last accessed 04/2023, Site Nos. 414411112543701 and 401312112442301), shown as green squares in Figure 1, have relatively comparable time samplings. These two wells are located near the seismic stations HVU and DUG (the green squares in Figure 1).

2.2. Temperature Data

In addition to hydrological components, thermoelastic effects also contribute to the dv/v seasonality (Fokker et al., 2024; Richter et al., 2014; Shen et al., 2024; Tsai, 2011). Across Utah, the average air temperature change over a year ranges from below zero to 40 degrees Celsius. To take temperature effects into account, we collect air temperature records from the Parameter-elevation Relationships on the Independent Slopes Model (PRISM) Gridded Climate Data (PRISM Climate Group, https://prism.oregonstate.edu/, last accessed 04/2023, Daly et al., 2008). The PRISM Climate Group gathers climate data from numerous monitoring networks, applies advanced quality control methods, creates spatial climate data sets to reveal both short-term and long-term climate patterns, and provides the PRISM, a 4 × 4 km gridded product. We extract the data from the points closest to our seismic stations. The temperature records at each station are generally similar, with the lowest temperatures typically occurring in early February and the highest around July, averaging between 20.4 and 28.4 degrees Celsius annually. We interpolated the temperature and hydrological data daily to compare them with the dv/v time series.

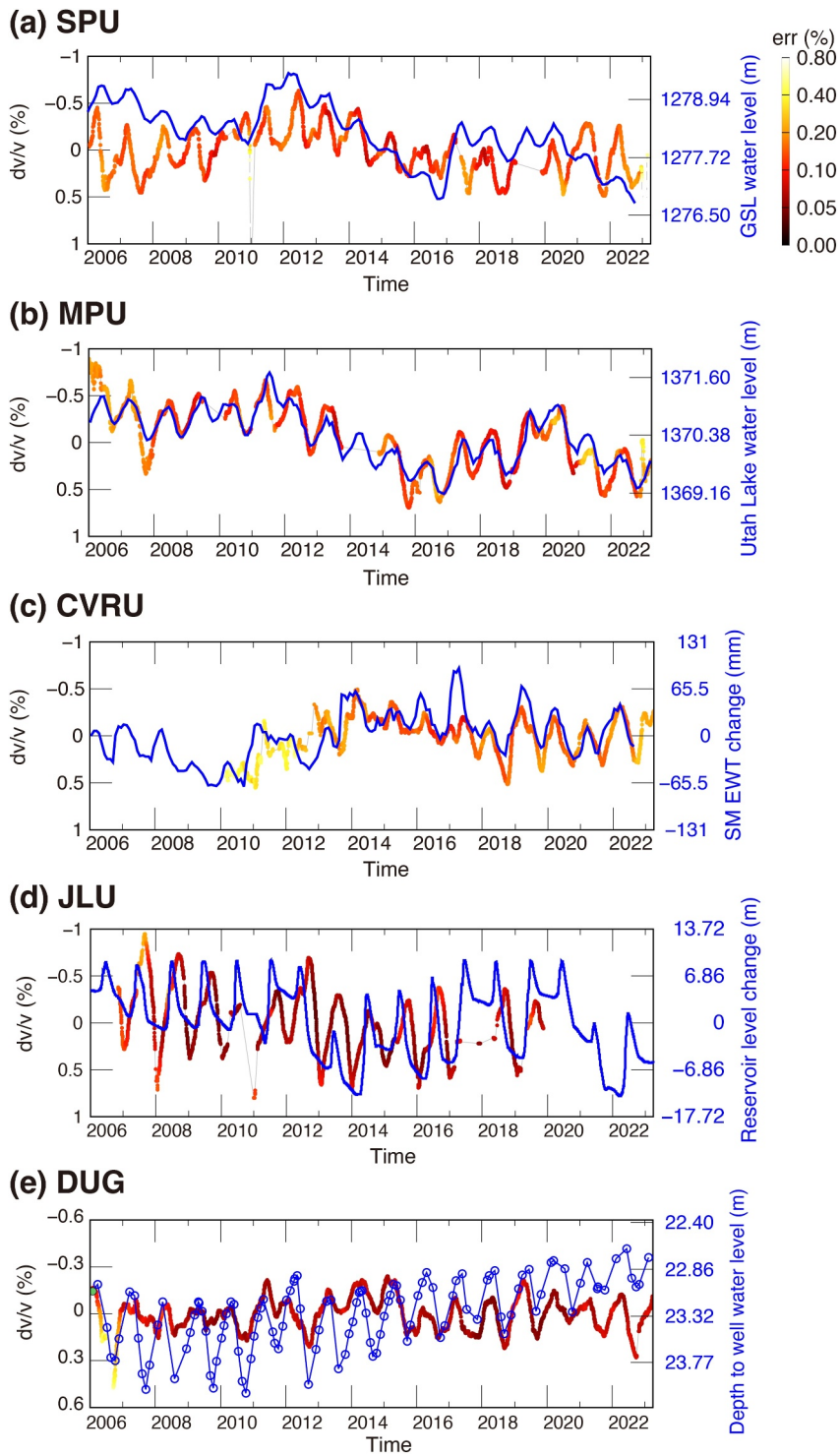

Figure 2. Temporal variability of observed dv/v (warm-color-coded curves) and the corresponding hydrological factors (blue curves). The dv/v axis is inverted in sign. (a) Station SPU dv/v versus the GSL level; (b) Station MPU dv/v versus the Utah Lake level; (c) Station CVRU dv/v versus the corresponding soil moisture equivalent water thickness (SM-EWT); (d) Station JLU dv/v and the Jordanelle Reservoir level; and (e) Station DUG dv/v and the nearby groundwater level record.

2.3. Seismic Data and Data Processing

Taking advantage of the continuous seismic recordings, this study analyzes three-component continuous broadband seismic recordings between January 2006 and March 2023 from the University of Utah Regional Seismic Network (UU) stations and the United States National Seismic Network (US) in Utah. To study both long-term and annual dv/v changes, we only include the 28 broadband stations with over 5 years of operation in our analysis (Figure 1, inverted triangles). Figure S1 in Supporting Information S1 shows data completeness for the stations. We perform a general standard pre-processing, which removes instrumental response, demeans, detrends, and tapers before decimating the data to 20 Hz and storing them in 1-day-long segments. We remove all component observations with data gaps in any single component and check daily waveforms in spectrograms to exclude malfunction periods.

2.3.1. Single-Station Cross-Component Correlations

We perform a single-station cross-component correlations (SC) analysis, which has been well demonstrated in investigating tectonically and environmentally driven dv/v evolutions in previous studies (e.g., Clements & Denolle, 2023; De Plaen et al., 2016; Feng et al., 2021; Hobiger et al., 2014; Viens et al., 2018; Yates et al., 2019). We adopt Welch's method (Seats et al., 2012) to improve the quality of the correlation functions. We first cut the daily three-component seismic data into 10-min windows, detrend, taper, and apply spectral whitening in the frequency band 0.1–8 Hz. We then calculate the SC functions between each non-identical component (i.e., ZN, ZE, NE, EN, EZ, and NZ) with non-overlapping 10-min time windows. We calculate the root mean square (RMS) amplitude for each 10-min SC and remove all 10-min SCs with an RMS above five times the daily averaged RMS. Those windows often contain unfavorable energetic signals (e.g., earthquakes, instrumental irregularities, and non-stationary transient signals). We stack all remaining SCs for each station and cross-component to obtain the references. The 60-day window is selected to obtain the coherence current SC functions (Figure S2 in Supporting Information S1). It enhances the coherence and retains essential signals across seasons. We focus on the 2–4 Hz frequency band, where coherent SC coda signals are observable.

2.3.2. Computing dv/v Using the Stretching Method

Assuming the velocity change in the medium is laterally homogeneous, for each 60-day stacked SC function (as the current SC function hereafter), we measure the relative velocity change dv/v compared to the reference SC function. Here, we assume that the dt/t (time shift over lag time) of the coda signal is related to dv/v via the equation (Snieder et al., 2002):

$$\frac{dt}{t} = -\frac{dv}{v}. \tag{1}$$

Equation 1 implies that delayed phase shifts ($dt > 0$) are associated with velocity reductions ($dv < 0$). For a uniform change in dv/v, the delay time increases with the lag time as propagation paths are longer for scattered waves that arrive later. We measure dv/v by band-passing the SC functions in the 2–4 Hz range and a selected 2–8 s lag time coda window (Figure S2 in Supporting Information S1, black boxes) to reduce the effect of energetic near-zero lag time ballistic waves.

We adopt the stretching method (Sens-Schönfelder & Wegler, 2006) to measure the dv/v evolution with time. A weighted contribution across the six SC components is used to compute the final dv/v time series, $\frac{dv}{v}_{final}$, (Hobiger et al., 2014; Viens et al., 2018):

$$\frac{dv}{v}_{final} = \frac{1}{\sum_{i=1}^{6} cc_i^2} \sum_{i=1}^{6} cc_i^2 \left(\frac{dv}{v}\right)_i, \tag{2}$$

where cc_i and $\left(\frac{dv}{v}\right)_i$ are the maximum correlation coefficients among the current and reference functions and the estimated dv/v of each component after stretching, respectively. We also calculate the uncertainty of the estimated dv/v for each cross-component following the approach of Weaver et al. (2011). We present the averaged uncertainty of all components as the uncertainty of our dv/v time series (e.g., Figure 2).

2.4. Spatial and Depth Sensitivity Measurements

The lateral sensitivity of our measurements is ∼1 km based on the first Fresnel zone approximation (Bennington et al., 2018). Assuming strong Rayleigh waves in the coda of the single-station correlations, we use surface-wave sensitivity with depth given a shear-wave velocity profile, taking the mean values from the grids near seismic stations from Schmandt et al. (2015) to obtain the depth sensitivity kernels as shown in Figure S3 in Supporting Information S1. With this framework, we find that the depth sensitivity of our measurements is within the top 150 m. This estimation carries some uncertainty since the velocity model may not accurately represent the near surface for assessing 2–4 Hz waves, and our assumption that surface waves dominate the SC (e.g., Yuan et al., 2021). The state's average water table depth is 8 m (Fan et al., 2007), though the UUSS broadband stations are mainly located away from the basins and where the water table is deeper (∼10–30 m). The satellite-based soil moisture SM-EWT provides estimates in the top 2 m (Xia, Mitchell, Ek, Sheffield, et al., 2012). These water-level depths are shallower and fall within the assumed depth of the seismic measurements, motivating our combined analysis of soil moisture and water table depth.

2.5. Modeling dv/v

We model dv/v with a linear combination of the factors to understand how much each factor contributes to the system. We identify two potential water storage mechanisms that impact seismic velocities: subsurface moisture (e.g., Illien et al., 2021; Oakley et al., 2021; Shen et al., 2024) and water-table levels (e.g., Gaubert-Bastide et al., 2022; Voisin et al., 2016). Furthermore, our satellite-based soil moisture observations are only sensitive to the top 2 m (Xia, Mitchell, Ek, Sheffield, et al., 2012). At the same time, the water table is reported to be below 3 m; we thus assume these observations are decoupled. The coupling between water table and SM-EWT may be expected during wet periods (e.g., Illien et al., 2021), but our measurements lack the sensitivity to discriminate between these components.

Additionally, we consider thermoelastic stress and model it with the time-shifted surface air temperature to model the diffusion at a depth of annual temperature variations (e.g., Berger, 1975; Richter et al., 2014). There could be confusion about residual seasonality in the groundwater level, because we removed seasonality (lowpass filtered) from our groundwater-level proxy using the lake level, which might leak into the thermoelastic term. A linear superposition is used as an approximation. Most studies on hydrological effects below the water table have assumed a linear superposition (Clements & Denolle, 2023; Ermert et al., 2023). Although recent work on partially saturated media suggests a more complex hydromechanical model (Sakaki et al., 2010; Shen et al., 2024; Solazzi et al., 2021) or discovers non-linear relationships between thermoelasticity and water content (e.g., Diewald et al., 2024), we ignore the more complex hydromechanical model and instead assume a linear relationship between soil moisture and dv/v, as previously used in the literature (e.g., Illien et al., 2021; Kang et al., 2025; Oakley et al., 2021).

2.5.1. Modeling dv/v

This study explores novel ways to introduce groundwater and soil moisture with temperature effects to explain seismic velocity variations, dv/v. First, we use a base model formulated as

$$\mathrm{dvv}_{\mathrm{base}}(t) = A + B \cdot \mathrm{SMEWT}(t) + C \cdot T(t - \Delta t_{\mathrm{tshift}}), \tag{3}$$

where the parameters to fit are the constant level (A) and coefficients (B, C) to respectively the soil moisture term, $\mathrm{SMEWT}(t)$ and the temperature term with a time shift $T(t - \Delta t_{\mathrm{tshift}})$. Considering the long-term decline of the groundwater table over the past decades (Perrone & Jasechko, 2017; Wada et al., 2010), we propose two models: (a) the base model in Equation 3 accompanied by a linear trend and (b) the base model in Equation 3 accompanied by a lowpass filtered lake level to synthesize water-table effects on dv/v. In the first model, a positive linear trend $\mathrm{LT}(t)$ represents the corresponding increase in dv/v due to the long-term decline in the groundwater table. The first model is written as

$$\mathrm{dvv}_{\mathrm{linear}}(t) = \mathrm{dvv}_{\mathrm{base}}(t) + \mathrm{LT}(t). \tag{4}$$

Table 1
Model Parameters and the Ranges Used for the MCMC Sampling

Variable	Description	Sampling range [min, max]
A	Offset of dv/v	[−1.0, 1.0]%
B	Factor of soil moisture equivalent water thickness	[−∞, 0]
C	Factor of temperature	[0, ∞]
Δt_{tshift}	Time shift of the temperature time series	[0, 90] days
D	Factor of the assumed groundwater level	[−∞, 0]
Δt_{wshift}	Time shift of the assumed groundwater level time series	[−182, 182] days
LT	Corresponding linear increase due to the linear decline of the groundwater table	[0, ∞]
f_0	Uncertainty of dv/v estimation	$[10^{-10}, 10^{10}]$

In the second model, assuming the regional groundwater level is similar to the lake level in the long term, we lowpass filter the Utah Lake level with a 2-year corner period to approximate the groundwater term denoted as $\text{Lake}_{\text{lowpass}}$ at any given time t, with a time shift Δt_{wshift} that allows for hydraulic diffusivity from the lake. The model leverages the known correlation between groundwater and lake levels (Namdar Ghanbari & Bravo, 2011; Wu et al., 2022), justified by the strong correlations between the GSL and the Utah Lake levels and dv/v (see Results section). This model is written as

$$\text{dvv}_{\text{lowpass}}(t) = \text{dvv}_{\text{base}}(t) + D \cdot \text{Lake}_{\text{lowpass}}(t - \Delta t_{\text{wshift}}), \tag{5}$$

where D is the sensitivity of the groundwater to dv/v.

2.5.2. Model Fitting With Bayesian Inference

Following the steps outlined by Ermert et al. (2023) and Okubo et al. (2024), we utilize emcee, a software tool based on Python (Foreman-Mackey et al., 2013), to fit the time series in a Bayesian framework. The emcee employs the MCMC method and offers various advanced sampling algorithms. The MCMC process is a Bayesian method for estimating model parameters by generating samples from posterior distributions when analytical solutions are lacking. It forms a Markov chain that explores the parameter space based on observed data likelihood and prior information, producing samples from the posterior. We adopt the stretch move method that Goodman and Weare (2010) introduced to update model parameters involving a set of walkers. We choose 32 walkers and perform 12,000 iterations, with 10% discarding as burn-in. The log-likelihood function, $\ln(l(\theta))$, with a set of model parameters θ is referred to as Okubo et al. (2024):

$$\ln(l(\theta)) = -\frac{1}{2}\sum_i \left[\frac{(\text{dvv}_{\text{obs}}(t_i) - \text{dvv}_{\text{model}}(t_i, \theta))^2}{\hat{\sigma}_i^2} + \ln(\hat{\sigma}_i^2) \right], \tag{6}$$

where σ_i is the estimated error of the observed dv/v, dvv_{obs} is the observed dv/v, and $\text{dvv}_{\text{model}}$ is the predicted dv/v from models $\text{dvv}_{\text{linear}}$ and $\text{dvv}_{\text{lowpass}}$ at the time t_i, respectively. During the modeling process, we set the prior values of each term based on the knowledge of previous literature, such as B and D are negative due to the anti-correlation between shear waves (dv/v) and water content (e.g., soil moisture in Illien et al., 2021; and groundwater level, Sens-Schönfelder & Wegler, 2006); C is positive due to the correlation between dv/v and air temperature (e.g., Richter et al., 2014). Table 1 summarizes the parameters and the corresponding sampling ranges of the model. The 90-day bounds of temperature effect are based on an average 70-day shift from a statewide experiment by Clements and Denolle (2023). The time shift of the assumed groundwater table is given in a range of [−182, 182] days, considering the unknown inflow and seepage (e.g., Somers & McKenzie, 2020), but only within a year-round cycle.

To prepare the data for modeling, we apply a 30-day rolling average to the dv/v time series to smooth it and make it comparable to other variables, such as SM-EWT, lake level, and temperature, all sampled monthly. We trim the

time series with the exact starting and ending dates to align each component at the same stations. All the time series have the mean values removed and have been normalized to [−1, 1]. Stations HVU and VRUT have over a year of data gaps, which will introduce biases into modeling processes. Therefore, we divided these data sets into two periods for these stations and named them HVU1, HVU2, VRUT1, and VRUT2.

Recent studies have proposed that coupling between soil moisture, groundwater, and temperature may be necessary to explain the dv/v time series better and to better represent rheological models (e.g., Diewald et al., 2024; Illien et al., 2021; Sens-Schönfelder & Eulenfeld, 2019). Since we lack in situ and independent information about these variables, we chose the simple model of decoupled, linear superposition of effects.

3. Results and Interpretation

3.1. Seasonality of the Observed dv/v

The observed dv/v evolutions reveal strong seasonality at most stations. We calculate yearly averaged dv/v time series at all stations to investigate the strength of their seasonality (Figure 3; see Figure S4 in Supporting Information S1 for all stations). Figure 3c shows the annual dv/v stacks for several representative stations. Based on the yearly dv/v variations, we calculate the average peak time of the highest and lowest dv/v for all stations and summarize them in Figures 3a and 3b. Considering the uncertainties of those low annual variation stations, we only showed those time series with average yearly variations above 0.3%. Overall, the average positive dv/v peak times are observed in autumn between August and October (Figure 3a), and the negative dv/v peak time appears around late spring and early summer between April and June (Figure 3b). These peak time patterns are consistent with Utah's general water cycle, which goes from October 1st to September 30th, where groundwater is lowest during the dry summer-fall months and replenishes during the spring runoff. Station JLU is unique due to its proximity to the managed reservoir. It is reasonable that it shows a different peak time than the others. Looking more closely, stations HWUT and FORU have a dv/v plateau during the autumn and winter months (Figure 3c) despite the peak times being slightly delayed compared to other stations (Figure 3). Stations at higher elevations tend to have a later negative peak time, likely due to the late snowmelt in mountainous areas, although this is not always apparent.

3.2. Basic Correlation Between dv/v and Lake Levels

The GSL and Utah Lake water level records manifest the multiyear dry-wet variations of the northern Utah hydrological system. The lake's water level reflects the 2007 drought and multiyear droughts in 2012–2017 and 2020–2022 (Figure 4a). Similar long-term variations are also observed by the dv/v at nearby stations in the GSL watershed (Figure 4b, those red inverted triangle stations in Figure 1). In Figure 4b, the dv/v time series are plotted in a negative sense to improve visualization of the anti-co-evolution of the water levels. We see a slight downgoing (increase in dv/v) in 2007 at Stations MPU and SPU. An apparent long-term decline (increase in dv/v) over the six stations appeared in 2012–2017 and the period after 2020.

The dv/v at stations within the GSL watershed generally correlate better with lake levels than stations outside. Figures 5a and 5b provide an overview of the correlation coefficients and R-squared values for each station listed in Table S1 in Supporting Information S1. Within the watershed, Station MPU demonstrates the strongest negative correlation to the water levels of both the GSL and Utah Lake, with values of −0.82 and −0.91, respectively. The significant correlation at Station MPU suggests that the dv/v measurement and the Utah Lake level are sensitive to the same hydrological factors. The two stations near the Salt Lake Valley between Utah Lake and the GSL (Stations CTU and NOQ) show stronger correlations with Utah Lake levels, with values of −0.69 and −0.58, and slightly lower correlations to the GSL of −0.59 and −0.4. The two stations near the GSL (Stations SPU and HVU) show slightly lower correlations with the lakes, with values between −0.42 and −0.65. Surprisingly, station BGU shows a stronger correlation with the Utah lake water level (−0.82) than with the GSL water level (−0.67). Station RDMU, outside the GSL watershed, shows a high correlation with the GSL water level (−0.72), higher than other outside-watershed stations.

3.3. Basic Correlation Between dv/v and SM-EWT

The correlation coefficients between dv/v and the SM-EWT show less spatial coherence (Figure 5c), unlike the correlation between lake water levels and dv/v, which is primarily focused within the GSL watershed. The

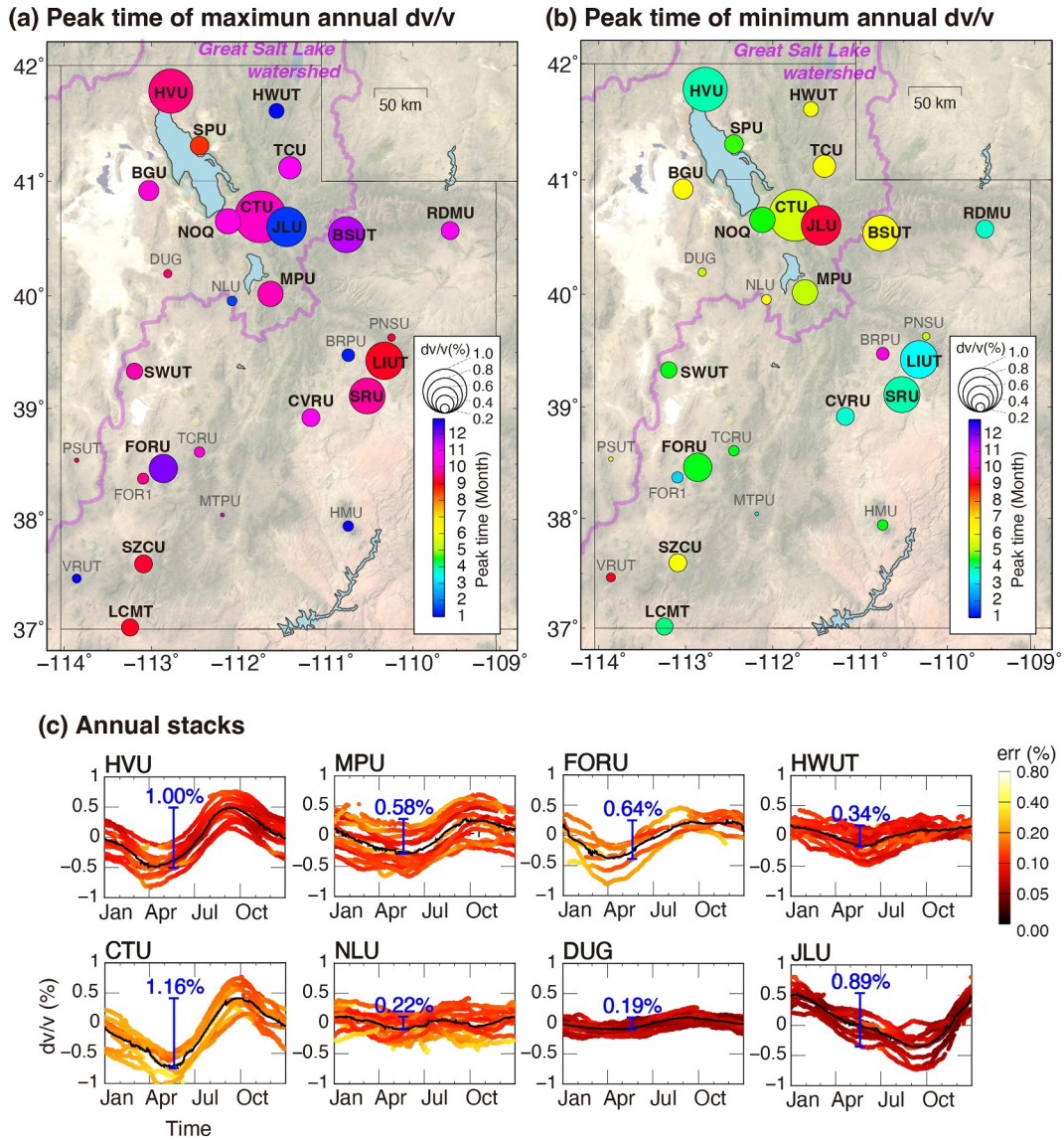

Figure 3. Peak time maps of the (a) highest and (b) lowest points in annual dv/v, and the (c) annual stacks. In (a) and (b), the circles are color-coded with the peak time, along with their average peak-to-peak annual variations presented by size. The pink line marks the Great Salt Lake watershed boundary. The peak-to-peak seasonal mean amplitudes are represented by their circle size. The stations with annual variation (larger than 0.3%) are noted in bold-texted station names.

strongest (anti-)correlation appears at Station CTU, with a value of −0.78 (highlighted by a yellow label in Figure 5c). The Stations FORU and FOR1 in southern Utah also show relatively high correlations of −0.72 and −0.6. Station CVRU (highlighted by an orange label in Figure 5c) is one of the few stations deployed on a soil site, as documented by the UUSS (Farrell, pers. comm.). While the correlation at CVRU isn't the strongest, its correlation coefficient reaches −0.56. Except for Station JLU, the correlation coefficients between dv/v and SM-EWT are mainly negative, consistent with previous findings (e.g., Illien et al., 2021; Shen et al., 2024). However, it is worth noting that we are not using direct soil moisture measurements; instead, we are comparing our results with the equivalent water thickness from NLDAS-2 that correlates best with in situ moisture relative to other remotely sensed measurements during this period.

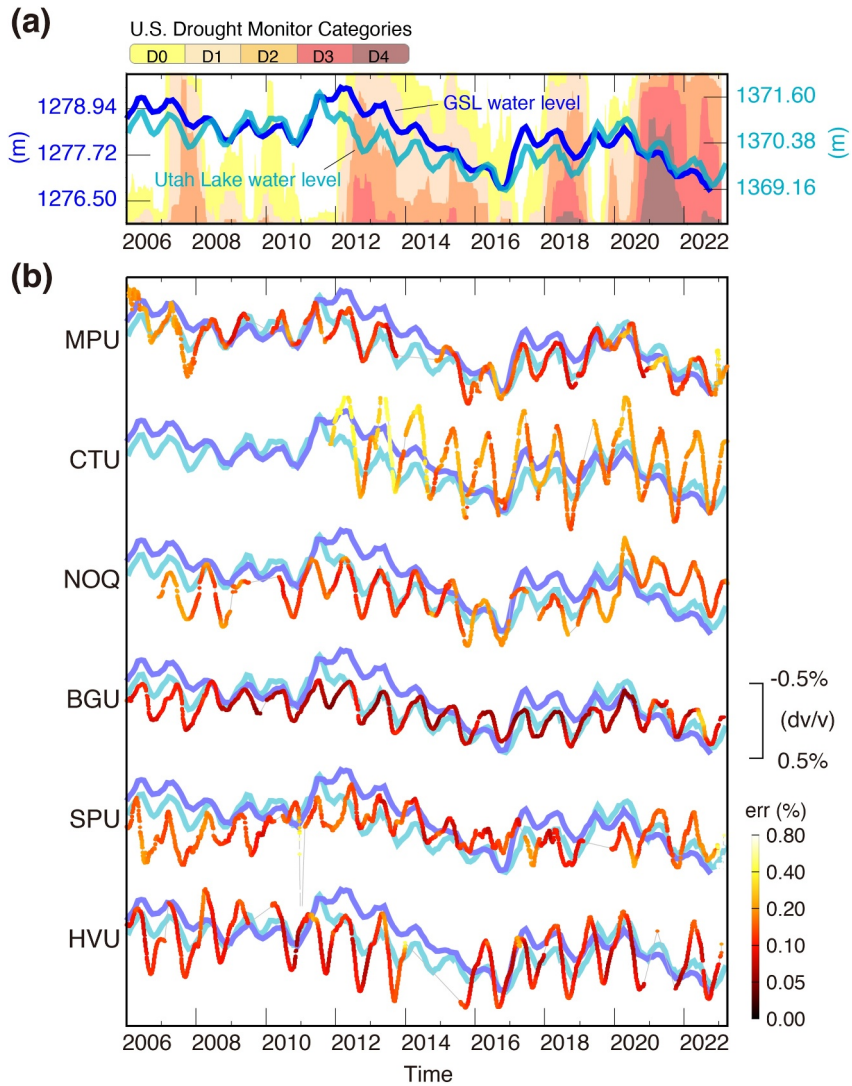

Figure 4. Co-evolution of dv/v and GSL and Utah Lake levels. (a) Lakes' water level variations with the drought monitoring graph from the US National Integrated Drought Information System; D0–D4 represent different drought levels, from abnormally dry (D0) conditions to exceptional drought (D4). The blue and cyan curves represent the GSL and Utah Lake records, respectively. (b) Co-evolution of flipped dv/v for stations adjacent to the lakes (red reversed triangles in Figure 1) and the lakes' water level records (same scale as in (a) and with slight transparency). The color of the dv/v curves represents estimated uncertainty.

3.4. Models of dv/v With All Factors

We explore the posterior distribution that arose from the MCMC inversion in Figure 6. Diagonal terms represent the marginal posterior distributions for individual model parameters, while the off-diagonal panels show the joint distributions between pairs of model parameters, highlighting their trade-offs. This result highlights the strength of the Bayesian MCMC approach in capturing the full range of plausible parameter values and their interdependencies, information that would be missed by relying solely on single-point estimates or best-fit models.

We evaluate the quality of models using the Akaike information criterion (AIC, Akaike, 1974) and the Bayesian information criterion (BIC, Schwarz, 1978), which were recently used in modeling dv/v time series (e.g., Okubo et al., 2024). These criteria assess the trade-off between goodness of fit and model complexity, penalizing the number of free parameters to avoid overfitting. AIC is based on information theory and favors models that balance fit and flexibility; lower AIC values indicate a better model. BIC introduces a stronger penalty for complexity that increases with sample size, making it more conservative and more likely to select simpler models when data are

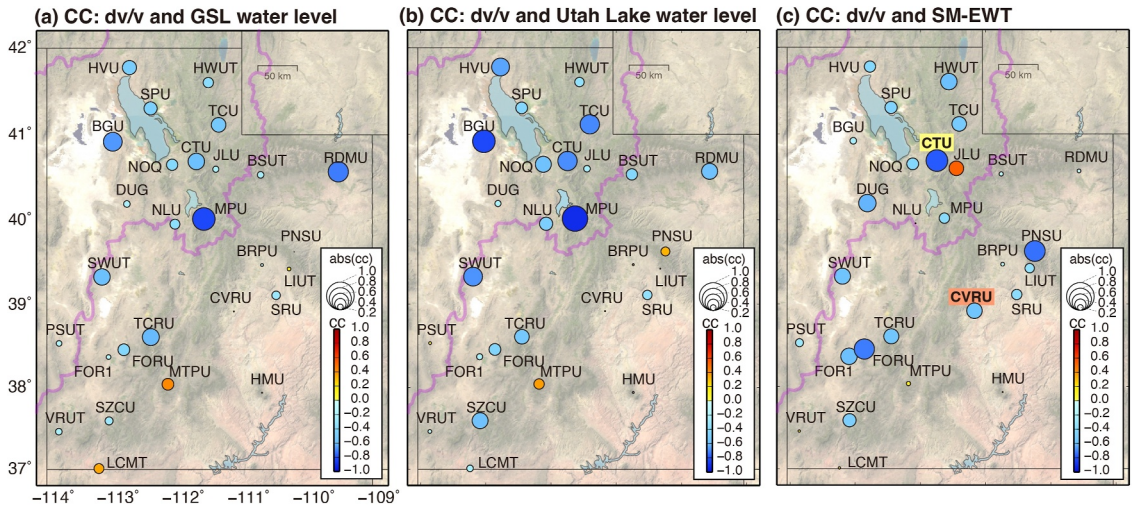

Figure 5. Correlation between the observed dv/v and the lakes' level variations and SM-EWT. (a) dv/v correlation with the GSL water level; (b) dv/v correlation with the Utah Lake water level; (c) dv/v correlation with SM-EWT. The colors represent the correlation coefficient between the dv/v and the corresponding lake water level. The circle size shows the absolute value of the correlation coefficient at stations. The pink lines in the figures represent the extent of the Great Salt Lake watershed.

plentiful. In addition to the two models mentioned in Section 2.5 (Equations 3–5), we also evaluate them by retaining only SM-EWT or temperature in both to assess their performance with one excluded. The number of model parameters, k, in the linear-trend and low-pass models mentioned in Section 2.5 is 5 and 6, respectively. When we retain only the SM-EWT term in the model, k is 3 and 4. When we retain only the temperature term with a time shift, k is 4 and 5. Overall, the combination of hydrological and thermoelastic terms provides a better fit.

We select the best fit of the testing models as the one with the highest likelihood. Figures S5, S6, and Table S2 in Supporting Information S1 summarize the optimal fits and their factor values. Here, we demonstrate the misfit of each model as well as the AIC and BIC analyses by using the difference between the model of the soil moisture term with a linear trend for illustration (Figure 7). The misfit and ΔAIC result (Figures 7a and 7b) suggest that the lowpass model (magenta points) provides a better explanation of the data for most stations. However, the ΔBIC results indicate that the lowpass model is not systematically the optimal choice for all stations. This discrepancy highlights the inherent bias in AIC toward more complex models and the more conservative nature of BIC. It also suggests that no single model can fully capture the observed behavior across all stations at distinct regimes, pointing to spatial variability in the controlling processes or data constraints.

Subplots (d) and (e) in Figure 8 illustrate the fitting results for both models at two example stations, MPU and SRU, alongside their input time series shown in subplots (a–c). At Station MPU, the long-term dv/v pattern is effectively captured and explained by the lowpass model. However, at some stations, the AIC and BIC values for different models are very close to each other, indicating that long-term water table decline is equally well represented by a simple linear trend as the groundwater table proxy. Some stations, such as HMU and NLU, exhibit poor model fitting altogether, with high misfit and high AIC-BIC values (see time series in Figures S7 and S8 in Supporting Information S1). Some stations exhibit equal model fitting, regardless of the model compositions, as indicated by similar AIC-BIC values (e.g., SRU, shown in Figure 7). Some stations see greater improvement when incorporating a more sophisticated model (e.g., the low-pass model) with lower AIC-BIC values and lower misfit, such as stations MPU and CTU in the Great Salt Lake Watershed.

4. Discussion

4.1. dv/v Variability and Local Site Conditions

The dv/v variability across stations may provide helpful information for understanding the regional hydrological processes in different parts of the State of Utah. While the annual dv/v amplitude of each station varies (Figure 3), stations in the south and west of the GSL (e.g., BGU and NOQ) show a relatively smaller value than the station at the north edge of the GSL (e.g., HVU). This pattern may be related to the underground aquifer structures, geological features, and lake inflows (Baskin et al., 2002). The dv/v observed at stations outside the GSL

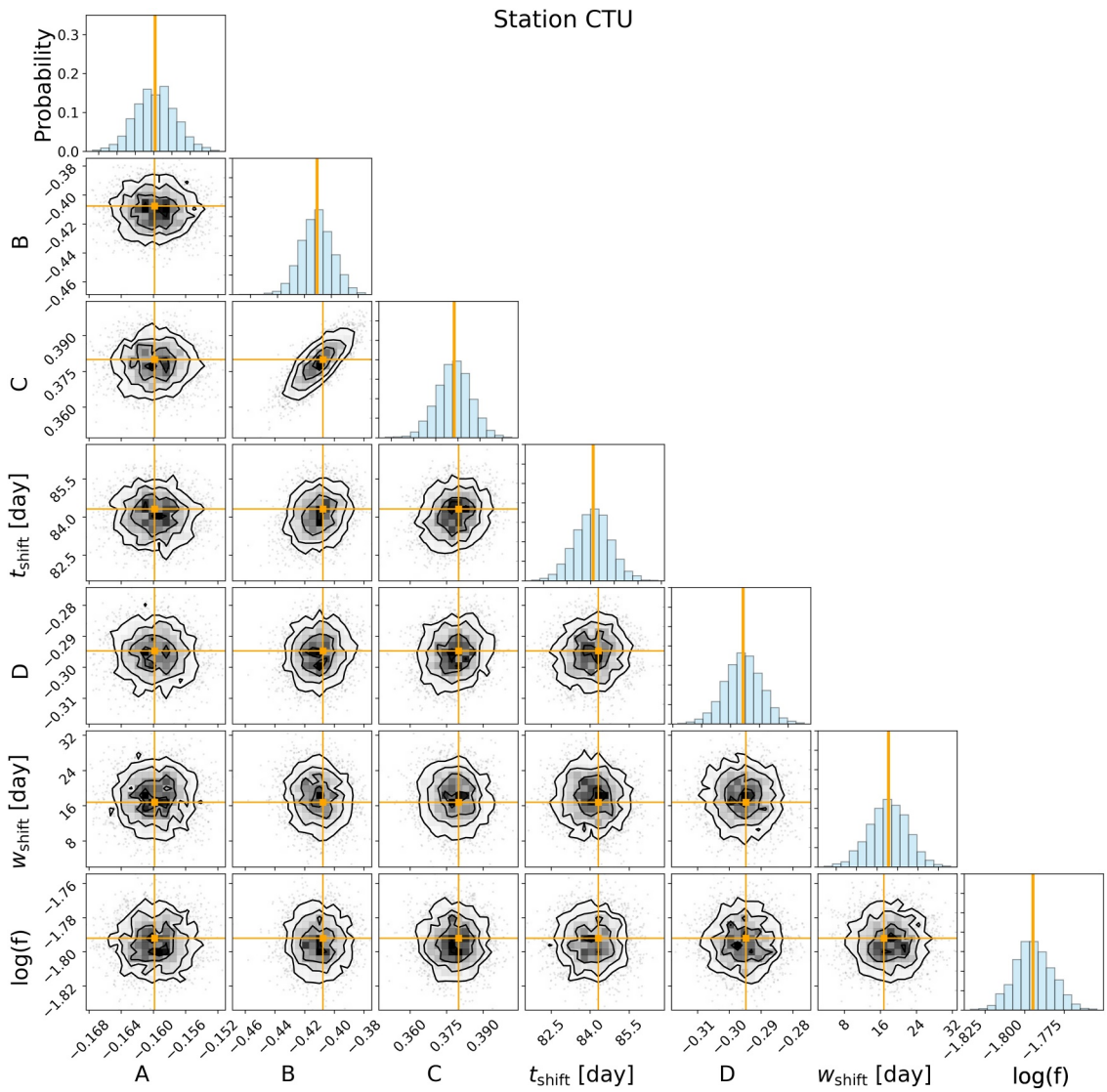

Figure 6. Posterior probability distributions of the model parameters derived from the MCMC analysis for Station CTU. The diagonal panels represent the probability mass functions, with bar sums normalized to one. Solid vertical lines indicate the best likelihood value, and the contours represent the 2D histogram of the model parameter pair, with darker colors signifying higher probabilities. Orange squares indicate optimal model parameters. Notably, the best likelihood parameters do not always align with the peaks of the probability distributions.

watershed has no spatial correlation. The latter may indicate that other controlling factors, such as rheological response or incorrect groundwater proxies, may hinder this analysis.

To further explore the lithological dependence on the dv/v variability, the soil type information obtained from the Utah Geospatial Resource Center (https://opendata.gis.utah.gov, last accessed 07/2024) and Vs30 values (Heath et al., 2020) at each station were collected and summarized in Table S3 in Supporting Information S1. Throughout the comparison, while no clear relationship was found between dv/v amplitude and soil type, annual temperature, or SM-EWT changes (Figure S9 in Supporting Information S1), a higher correlation (0.61) was observed with Vs30, indicating that seismic characteristics may play a role.

4.2. (No) Regional Pattern

Utah has a semi-arid, desert overall climate with microclimates influenced by topography and surface water bodies. The hydrological year typically begins when precipitation returns after a dry summer, usually on October 1st. The regional weather pattern shows that fall and winter bring precipitation, particularly heavy winter snow.

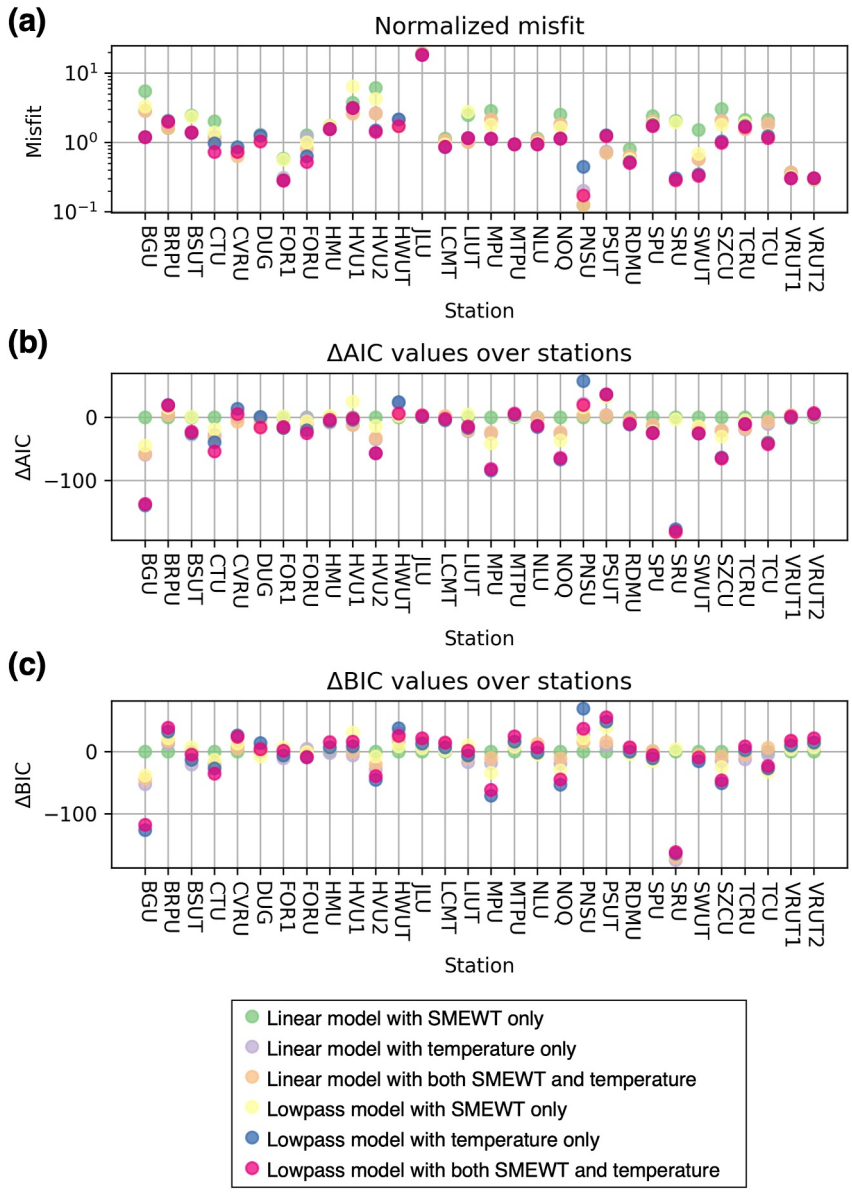

Figure 7. The (a) normalized misfit, (b) ΔAIC, and (c) ΔBIC values across stations. ΔAIC and ΔBIC are calculated by subtracting the values from the linear model with SM-EWT only. The colors indicate the models, each with different components involved.

Snowpack melt gradually replenishes the surface and groundwater in winter and spring. Surface and groundwater storage (e.g., reservoirs and aquifers) recharge in the spring and deplete over the summer due to high air temperatures (evaporation and groundwater usage) and low precipitation.

The annual dv/v cyclicity typically begins with a decline in late September and early October (Figure 3), which aligns well with the start of hydrological year cycles. This decrease in dv/v continues until the following April and May, reaching its lowest point, which may indicate the highest groundwater level or near-surface water content. After that, dv/v increases until the fall, and the cycles repeat. Snowmelt, the primary source of stream and groundwater replenishment in the Mountain West, may correspond with the peak of dv/v stacks.

Additional quantitative interpretations are difficult to draw from the lack of spatial patterns. We do not observe a clear relationship between the lowest or highest dv/v and site conditions: correlation is weak among elevation, slope, and aspect, given the location of the sensors and a 30 s (~1 km) Digital Elevation Map, for which we chose

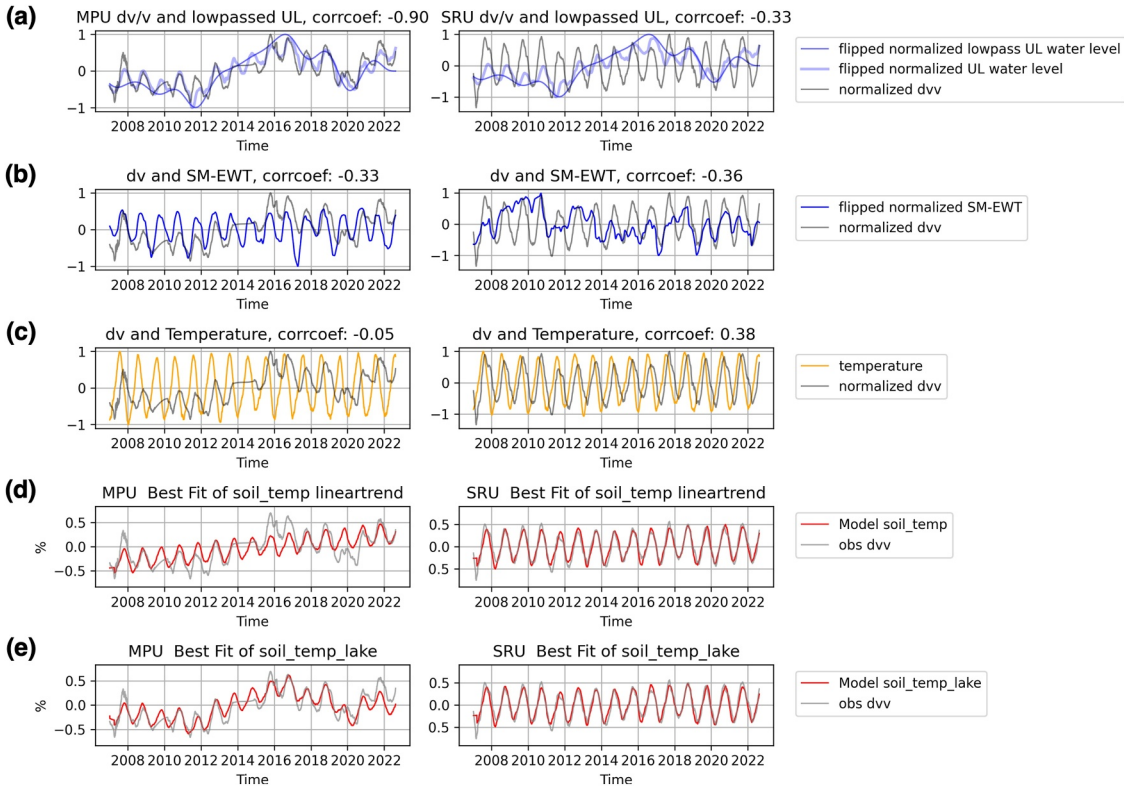

Figure 8. The modeling of the time series of Stations MPU and SRU. The subplots from top to bottom are the normalized terms used in the model fitting process: the normalized dv/v (gray curves), (a) flipped Utah Lake water level (thin blue curves) and lowpass lake water level (thick blue curves), (b) flipped SM-EWT (dark blue curves), (c) temperature records (orange curves), and (d) the optimal fit of the linear-trend and (e) lowpass models (red curves).

SRTM15+V2.6 from Tozer et al. (2019). We only found a weak anticorrelation (−0.24) between the time of maximum dv/v (lowest groundwater levels) and the slope, which we interpret as earlier depletion in the mountainous areas where snow melts and flows to the plains, and delayed aquifer discharge in the plains.

The co-evolution of observed dv/v and water levels between the GSL and Utah Lake (Figure 4) demonstrates regional seismic stations' resolvability to monitor water resources in watersheds. Utah Lake is located upstream of the GSL, connected by the Jordan River. A stronger correlation between dv/v and Utah Lake water levels is observed. It is possible that GSL's water level is not the most suitable groundwater proxy, as it is subject to strong summer evaporation and more affected by anthropogenic activities and agricultural groundwater usage. Therefore, some stations' dv/v have higher correlation coefficients with the Utah Lake water level than with the GSL.

We recognize that we are not solving for the water budget, which would entail balancing inputs of rain precipitation, snowmelt, lake seepage, with outputs of evapotranspiration, and runoff, to estimate soil moisture and groundwater table, because we are not modeling these terms due to complex coupling with the atmosphere. For example, air temperature controls the evaporation from surface water and moisture in the vadose zone (i.e., Benson & Dirmeyer, 2021; Chen et al., 2020). Our simplified model of anticorrelation between water storage and dv/v is empirical but well supported by past observations (e.g.,Clements & Denolle, 2018; Illien et al., 2021; Mao et al., 2025; Sens-Schönfelder & Wegler, 2006; Shen et al., 2024). However, our novel contribution that most seismic station dv/v are better explained by a combination of groundwater and subsurface moisture, is important.

4.3. What Is the Dominant Effect on dv/v?

The coefficients that optimally fit the lowpass model are markers of the relative significance between individual contributors to the temporal evolution of dv/v (Figure S6 in Supporting Information S1). Coefficient *B*, related to the relative importance of subsurface soil moisture, shows a spatial pattern similar to the dv/v-moisture correlation (Figure 5c), as expected from the strong correlation. Stations that are more sensitive to soil moisture

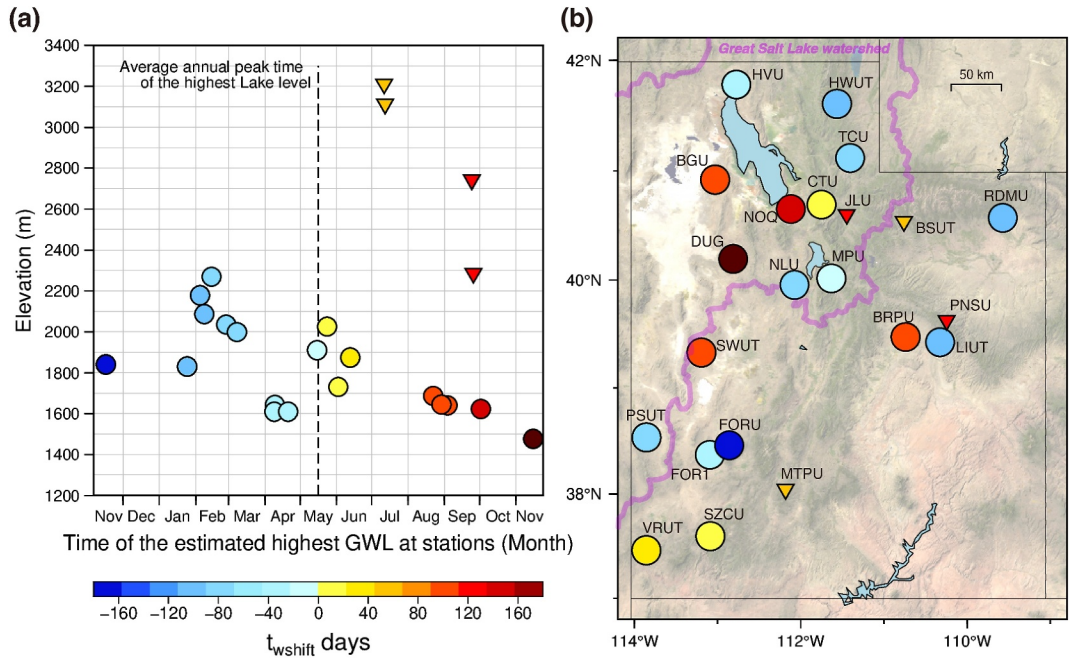

Figure 9. The distribution of the best Δt_{wshift} relative to the (a) station elevation and (b) station locations. The circles represent the stations with relatively low elevations (separate two clusters in (a)) compared to stations with relatively high elevations (triangles).

somewhat exhibit lower Vs30 values, likely explained by the fact that lower velocities increase shallow depth sensitivities for dv/v. Since the broadband stations used in this study are intentionally deployed on bedrock sites, where high Vs is expected near the site, the weak correlation may be related to uncertainty in the Vs30 model or in selecting Vs30 as a proxy for the Vs structure at the entire site.

There is no specific spatial pattern for the significance of thermoelastic effects, as measured by C, the importance of thermoelastic effects, and Δt_{tshift}, the phase shift for thermoelastic stress related to the thermal diffusion properties of the materials. This indicates that we cannot draw a physical interpretation to predict common thermoelastic effects at these sites. Because our goal was to characterize hydrological effects, we treat it as a correction in the later analysis, rather than interpreting its physical meaning.

The pattern in water table level proxy, indicated by coefficient D (i.e., lake level), shows a spatial coherence among those sites within the GSL watershed, especially along the mountain front. The time shift to the water table proxy, Δt_{wshift}, reflects the phase difference between the local water table and the proxy water level. A group of stations shows unsatisfactory results when fitting with the best-found time shift, 19 stations (shown as circles in Figure 9) that exhibit a strong anti-correlation between the Δt_{wshift} and elevation (CC = −0.64, Figure 9a). The trend can be explained by the gravitational flow from the high-elevation snowmelt-recharged water table down to the valley floor and that is well described in the Mountain Block Recharge (MBR) model (Markovich et al., 2019) The presence of positive Δt_{wshift} values may indicate that these sites exhibit water-level high after the lake is recharged, which could be explained by the fact that the lake recharge is much faster from rivers than from groundwater, and that groundwater recharge may be slower from the foothills and/or partially explained by lake seepage. We interpret from our modeling that the groundwater levels peak from January to March at high elevations and then from August to November on the valley floors. We thus interpret that the recharge is quite heterogeneous, with some areas in the state clearly lagging behind surface water recharge. This implies a long-term gravity-driven flow that may be around 19.2 m/month, similar to what is reported for MBR (Markovich et al., 2019).

At some sites, the groundwater table peaks at some stations earlier than the general snowmelt season, which we explain by early snowmelt in winter and spring. Note that the high-elevation stations that follow the trend are still lower than those stations out of the trend (triangles in Figure 9), likely because they are situated at elevations

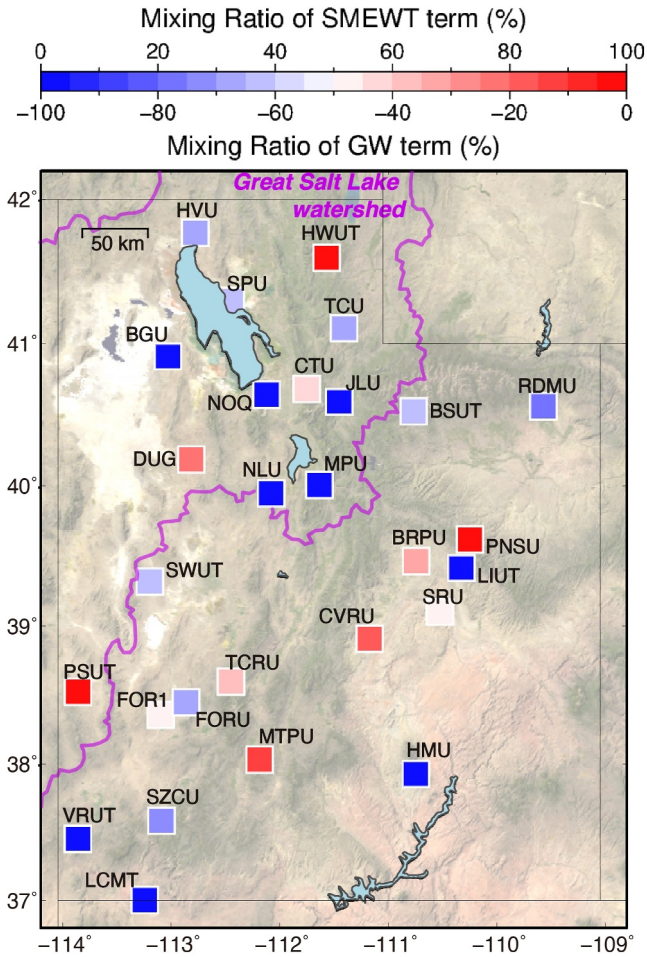

Figure 10. The mixing ratio map between the SM-EWT and GWL terms that explains the hydrological signal of dv/v. When the SM-EWT term dominates in fitted dv/v, the stations are color-coded red. When the groundwater term dominates, the stations are color-coded in blue.

where snowpack accumulated more over the winter. We excluded several stations from this MBR phase analysis because their best time shift posterior distributions were found at the boundary of our prior. Some of them show weak annual variations (e.g., VRUT). Some are strongly correlated with thermoelastic effects (e.g., SRU), subsurface moisture (e.g., CVRU), or other water bodies (e.g., JLU). Several stations are outside the GSL watershed and at higher elevations than the network average (e.g., BSUT, PNSU, MTPU).

An additional measure of hydrological contribution to dv/v can be determined by the relative contributions between soil moisture and water table in explaining dv/v, we calculate the mixing ratios $R_{\mathrm{SMEWT}} = -B/(|B| + |D|)$ and $R_{\mathrm{GW}} = D/(|B| + |D|)$, respectively (Figure 10). The mixing ratio spatial pattern indicates that the groundwater levels contributes greatly to dv/v at the stations within the GSL watershed, but the lack of spatial pattern can easily be drawn from sites outside of the watershed.

Our approach of applying a low-pass filter to the lake levels enables us to observe the rises and falls of the groundwater table over a long-term scale. The residuals between the optimal model and observations can likely be attributed to the shorter timescale groundwater level variations, which we ignored in this work, or residual soil moisture content (Dralle et al., 2018; Illien et al., 2021; Padilla et al., 2014). Another possible factor contributing to the mixing ratios is the velocity structure below the stations. Although our measurements suggest a top 150-m depth sensitivity, the various velocity structures at stations may also contribute to either moisture, which samples shallower perturbations more effectively, or the groundwater table, where relatively deeper perturbations are present.

These patterns demonstrate site dependency and local dv/v uniqueness. Figure 11 conceptually illustrates the findings in this study. Seismic stations near the lake or on the arid plain capture different environmental processes that induce diverse rheological responses (dv/v). Each station has different contributing terms for modeling, making it difficult to draw general behavior from this data, a finding which is quite similar to that of previous studies (Clements & Denolle, 2023; Viens et al., 2018). Our modeling results suggest that while the groundwater table has generally declined over the past decades, using lake levels as proxies for the groundwater table effectively estimates groundwater flow time and length scales confirming that downstream lake levels as a proxy for local groundwater (e.g., hydropotential) seems well justified and aligns with our seismic observations.

4.4. The Observed dv/v and In Situ Groundwater Well Data

At Station DUG, the dv/v time series shows a modest correlation (−0.39) with groundwater level variations recorded at a nearby well, despite the station being only ∼6.8 km away. Given the expected lateral sensitivity of dv/v measurements (∼1 km), this distance may still be too far to capture localized hydrological changes. Additionally, site-specific factors such as differing water usage or recharge conditions could influence the well measurements, contributing to the lower correlation. DUG is located at a surface-water divide (Markovich et al., 2019), which might explain the modest correlation with the well measurements.

In contrast, Station HVU, located approximately 12.3 km from a groundwater well, demonstrates a considerably stronger correlation (−0.69) between dv/v and groundwater level variations during 2010–2022 (Figure S10 in Supporting Information S1). Aside from a lag of ∼1.4 months, the time series are well aligned, likely reflecting the spatial offset between the seismic and hydrological sites. This strong agreement indicates that passive seismic interferometry can effectively capture near-surface hydrological variations and may hold promise for groundwater monitoring, especially if applied with denser, locally distributed seismic arrays. This well is located downstream of the topographic high, where HVU is, supporting the strong hydraulic connection between the two sites and the complementarity of using seismic stations for groundwater well.

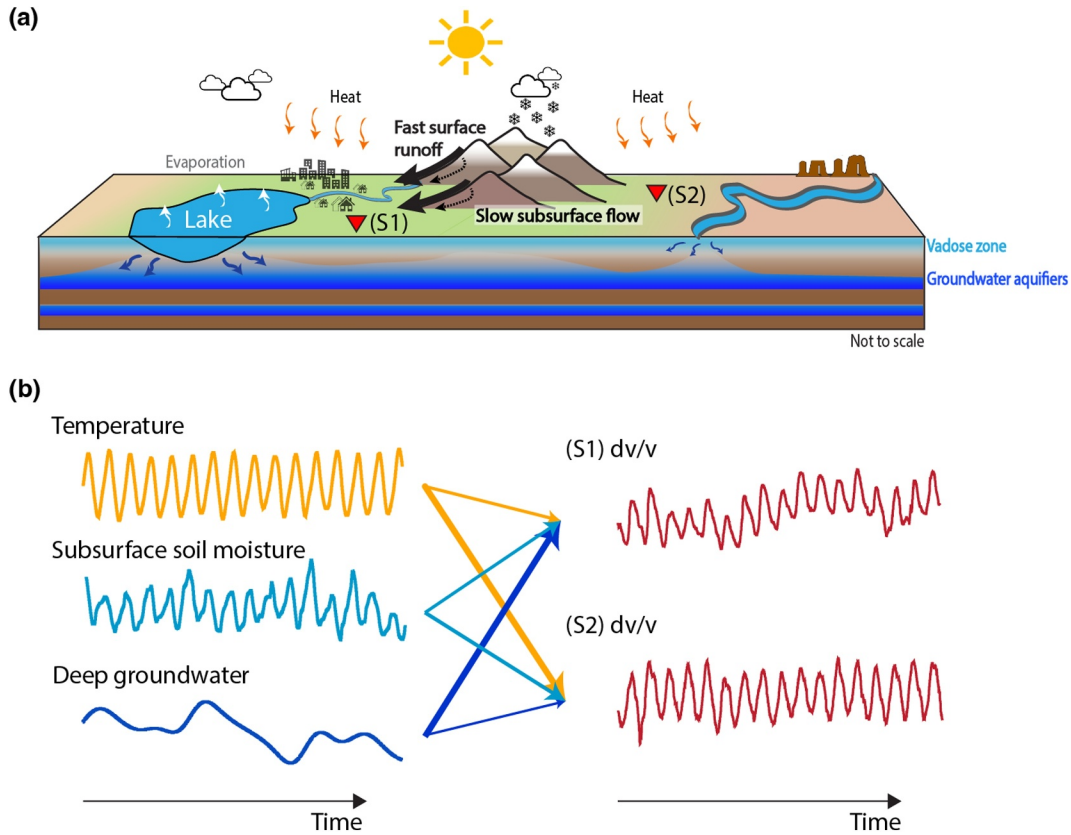

Figure 11. A conceptual illustration. A conceptual illustration of the near-surface seismic velocity response to hydrological and thermal forcing across a diverse landscape in Utah, based on findings in this study. (a) A schematic illustration of a diverse landscape with a cross-section. The cross-section depicts a simplified underground structure with vadose zones and aquifers. Seismic stations (S1 near the lake; S2 on the arid plain) capture distinct dv/v responses to local hydrological forcing. The thick black arrows represent the fast surface runoff, and the thin black dashed-line arrows represent the slow subsurface flow. (b) The schematic of the fitting components, temperature (orange), subsurface soil moisture (cyan), and deep groundwater variations (blue), which are linearly combined to explain observed dv/v signals (red curves) at each station. The arrow size represents the concept of how much each factor contributes.

4.5. The dv/v Response to Large Fluctuations of a Nearby Reservoir

Station JLU is severely affected by water levels in the Jordanelle Reservoir, exhibiting behavior distinct from other stations (Figure 2d). The two models proposed in Section 2.4 do not fit the observation at Station JLU at all (Figure S5 in Supporting Information S1). It implies that the primary factor driving dv/v here is the other major hydrological component, the reservoir. Therefore, we test another model using the base model $y_{\text{base}}(t)$ and reservoir water level with time shifting allowed in a range of [−182, 182] days, finding a well-converged solution with a shift of 49.5 days. The fitting results (Figure S11 in Supporting Information S1) are improved, although the model is still unable to fit the data very well. We note that the water level variation in Jordanelle Reservoir (Figure 2d) is considerable, about an order of magnitude greater than that of GSL and Utah Lake. Considering the relatively small surface area of the reservoir (~10 km^2), the dv/v variation of JLU might hence reflect the subsurface pore pressure response to a point water source (i.e., similar to a hydrological slug test but on a large scale).

5. Conclusions

We used time-lapse passive seismic interferometry to examine the near-surface hydrological processes through continuous seismic observation. We conducted a series of analyses on continuous seismic recordings from 28 broadband seismic stations across Utah State, covering the period between January 2006 and March 2023. We applied a single-station method to determine the temporal evolution of dv/v. Our dv/v findings uncovered distinct seasonality and long-term variations across the stations. We explored these dv/v patterns by comparing the

observed dv/v evolutions with two major surface water bodies in this area (i.e., the GSL and Utah Lake) and near-surface water (i.e., SM-EWT).

Throughout the analyses, we found that the average annual dv/v variations and peak times closely align with the state's regional water cycle, offering valuable insights into connecting near-surface seismic properties with hydrological processes. The amplitude in dv/v seasonality may be primarily related to local site conditions, as the Vs30 at the stations. Multi-year wet-dry cycles are captured by those stations within the GSL watershed. The strong correlation between dv/v and groundwater level, with lake levels serving as proxies and hydropotential surfaces, suggests that both are sensitive to the same controlling factors. Later, we examine the dv/v evolution using two linear models. We test two distinct groundwater level assumptions to account for the long-term declines in groundwater over the years. The modeling results suggest that a linear trend is too simplistic to estimate the pattern of the declining groundwater table. We take a lowpass filtered lake level as the assumption of long-term groundwater table variations in the model. Overall, this model gives a better explanation of dv/v.

This study highlights the feasibility of monitoring and understanding hydrological processes in semi-arid regions using time-lapse passive seismic interferometry. With ongoing climate change, it is crucial to implement effective management strategies that ensure the sustainable use of resources for both society and the environment. A major limitation of this study, also pointed out in Clements and Denolle (2023), is the challenging lack of spatial correlation between dv/v given the sensor spacing, which also highlight the spatial variability in groundwater flow and soil moisture. Further studies should build stronger hydrological models to establish if the observed spatial heterogeneity is explained by the spatial heterogeneity of the subsurface water and its dynamics over seasons.

Conflict of Interest

The authors declare no conflicts of interest relevant to this study.

Data Availability Statement

The Great Salt Lake water level data is from the USGS Water Resources (Site No. 10010100, https://waterdata.usgs.gov/nwis/dv?cb_62614=on&format=gif_default&site_no=10010100&legacy=&referred_module=sw&period=&begin_date=2006-01-01&end_date=2023-03-31). The two groundwater well records are from the USGS-Utah Water Science Center (Site Nos. 414411112543701, https://waterdata.usgs.gov/nwis/dv?cb_72019=on&format=gif_default&site_no=414411112543701&legacy=&referred_module=sw&period=&begin_date=2006-01-01&end_date=2023-03-31, and 401312112442301, https://waterdata.usgs.gov/nwis/dv?cb_72019=on&format=gif_default&site_no=401312112442301&legacy=&referred_module=sw&period=&begin_date=2006-01-01&end_date=2023-03-31). The Utah Lake data is from the Snowpack Telemetry Network (SNOTEL, Utah reservoir site 10166500, https://wcc.sc.egov.usda.gov/reportGenerator/view/customSingleStationReport/monthly/start_of_period/10166500:UT:BOR%257Cid=%2522%2522%257Cname/2006-01-01,2022-12-31/RESC::value,RESC::median_1991,RESC::pctOfMedian_1991?fitToScreen=false) maintained by the Natural Resources Conservation Service, U.S. Department of Agriculture (USDA). The soil moisture equivalent water thickness data is from the North American Land Data Assimilation System project phase 2 (NLDAS project, 2022). The Jordanelle Reservoir water level data is from the United States Bureau of Reclamation (https://data.usbr.gov/catalog/2353/item/471). The air temperature data is from the Parameter-elevation Relationships on the Independent Slopes Model (PRISM) Gridded Climate Data (https://prism.oregonstate.edu/explorer/map.php). The soil characteristics are derived from the Utah Geospatial Resource Center (https://opendata.gis.utah.gov/datasets/047e5268bed7404e8b7cf349d36c8283_0/explore?location=39.344336%2C-111.365547%2C-1.00). The seismic waveform data is from the IRIS data services. Data of noise correlation functions and post-processing scripts are available on Harvard Dataverse (Feng, 2024) and GitHub (https://github.com/kuanfufeng/Utah_Paper).

Acknowledgments
This work was supported by the Ministry of Science and Technology of Taiwan (Grant 111-2917-I-564-008) and the National Science Foundation of the US under award number OAC-2103701 and Grant EAR-1753362. Figures are produced using Generic Mapping Tools (GMT, Wessel et al., 2019) and Matplotlib (Hunter, 2007). We perform a Python tool *disba* (Luu, 2021, Computer software, https://doi.org/10.5281/zenodo.5775195), to obtain the depth sensitivity kernels. We thank the associate editor, Dr. Stefania Tarantino, and an anonymous reviewer for their careful review and constructive comments, which have helped improve the work.

References

Akaike, H. (1974). A new look at the statistical model identification. *IEEE Transactions on Automatic Control*, *19*(6), 716–723. https://doi.org/10.1109/TAC.1974.1100705

Baskin, R. L., Waddell, K. M., Thiros, S. A., Giddings, E. M., Hadley, H. K., Stephens, D. W., & Gerner, S. J. (2002). Water-quality assessment of the Great Salt Lake basins, Utah, Idaho, and Wyoming: Environmental setting and study design. USGS Report, 104. https://doi.org/10.3133/wri024115

Baxter, B. K., & Butler, J. K. (2020). Climate change and Great Salt Lake. In *Great Salt Lake biology: A terminal lake in a time of change* (pp. 23–52). https://doi.org/10.1007/978-3-030-40352-2_2

Bennington, N., Haney, M., Thurber, C., & Zeng, X. (2018). Inferring magma dynamics at Veniamin of Volcano via application of ambient noise. *Geophysical Research Letters*, *45*(21), 11–650. https://doi.org/10.1029/2018GL079909

Benson, D. O., & Dirmeyer, P. A. (2021). Characterizing the relationship between temperature and soil moisture extremes and their role in the exacerbation of heat waves over the contiguous United States. *Journal of Climate*, *34*(6), 2175–2187. https://doi.org/10.1175/JCLI-D-20-0440.1

Berger, J. (1975). A note on thermoelastic strains and tilts. *Journal of Geophysical Research*, *80*(2), 274–277. https://doi.org/10.1029/JB080i002p00274

Brooks, P. D., Gelderloos, A., Wolf, M. A., Jamison, L. R., Strong, C., Kip Solomon, D., et al. (2021). Groundwater-mediated memory of past climate controls water yield in snowmelt-dominated catchments. *Water Resources Research*, *57*(10), e2021WR030605. https://doi.org/10.1029/2021WR030605

Chen, X., Li, Y., Chau, H. W., Zhao, H., Li, M., Lei, T., & Zou, Y. (2020). The spatiotemporal variations of soil water content and soil temperature and the influences of precipitation and air temperature at the daily, monthly, and annual timescales in China. *Theoretical and Applied Climatology*, *140*(1–2), 429–451. https://doi.org/10.1007/s00704-020-03092-9

Clements, T., & Denolle, M. A. (2018). Tracking groundwater levels using the ambient seismic field. *Geophysical Research Letters*, *45*(13), 6459–6465. https://doi.org/10.1029/2018GL077706

Clements, T., & Denolle, M. A. (2023). The seismic signature of California's earthquakes, droughts, and floods. *Journal of Geophysical Research: Solid Earth*, *128*(1), e2022JB025553. https://doi.org/10.1029/2022JB025553

Coumou, D., & Rahmstorf, S. (2012). A decade of weather extremes. *Nature Climate Change*, *2*(7), 491–496. https://doi.org/10.1038/nclimate1452

Daly, C., Halbleib, M., Smith, J. I., Gibson, W. P., Doggett, M. K., Taylor, G. H., et al. (2008). Physiographically sensitive mapping of climatological temperature and precipitation across the conterminous United States. *International Journal of Climatology: A Journal of the Royal Meteorological Society*, *28*(15), 2031–2064. https://doi.org/10.1002/joc.1688

Delouche, E., & Stehly, L. (2023). Seasonal seismic velocity variations measured using seismic noise autocorrelations to monitor the dynamic of aquifers in Greece. *Journal of Geophysical Research: Solid Earth*, *128*(12), e2023JB026759. https://doi.org/10.1029/2023JB026759

De Plaen, R. S., Lecocq, T., Caudron, C., Ferrazzini, V., & Francis, O. (2016). Single-station monitoring of volcanoes using seismic ambient noise. *Geophysical Research Letters*, *43*(16), 8511–8518. https://doi.org/10.1002/2016GL070078

Diewald, F., Denolle, M., Timothy, J. J., & Gehlen, C. (2024). Impact of temperature and relative humidity variations on coda waves in concrete. *Scientific Reports*, *14*(1), 18861. https://doi.org/10.1038/s41598-024-69564-4

Donaldson, C., Winder, T., Caudron, C., & White, R. S. (2019). Crustal seismic velocity responds to a magmatic intrusion and seasonal loading in Iceland's Northern Volcanic Zone. *Science Advances*, *5*(11), eaax6642. https://doi.org/10.1126/sciadv.aax6642

Dralle, D. N., Hahm, W. J., Rempe, D. M., Karst, N. J., Thompson, S. E., & Dietrich, W. E. (2018). Quantification of the seasonal hillslope water storage that does not drive streamflow. *Hydrological Processes*, *32*(13), 1978–1992. https://doi.org/10.1002/hyp.11627

Ermert, L. A., Cabral-Cano, E., Chaussard, E., Solano-Rojas, D., Quintanar, L., Morales Padilla, D., et al. (2023). Probing environmental and tectonic changes underneath Mexico City with the urban seismic field. *Solid Earth*, *14*(5), 529–549. https://doi.org/10.5194/se-14-529-2023

Fan, Y., Miguez-Macho, G., Weaver, C. P., Walko, R., & Robock, A. (2007). Incorporating water table dynamics in climate modeling: 1. Water table observations and equilibrium water table simulations. *Journal of Geophysical Research*, *112*(D10). https://doi.org/10.1029/2006JD008111

Feng, K. F. (2024). Single-station cross-correlation functions of the broadband stations in Utah (2006–2022) [Dataset]. *Harvard Dataverse*. https://doi.org/10.7910/DVN/YCAAS4

Feng, K. F., Huang, H. H., Hsu, Y. J., & Wu, Y. M. (2021). Controls on seasonal variations of crustal seismic velocity in Taiwan using single-station cross-component analysis of ambient noise interferometry. *Journal of Geophysical Research: Solid Earth*, *126*(11), e2021JB022650. https://doi.org/10.1029/2021JB022650

Fokker, E., Ruigrok, E., Hawkins, R., & Trampert, J. (2021). Physics-based relationship for pore pressure and vertical stress monitoring using seismic velocity variations. *Remote Sensing*, *13*(14), 2684. https://doi.org/10.1093/gji/ggz228

Fokker, E., Ruigrok, E., & Trampert, J. (2024). On the temperature sensitivity of near-surface seismic wave speeds: Application to the Groningen region, the Netherlands. *Geophysical Journal International*, *237*(2), 1129–1141. https://doi.org/10.1093/gji/ggae102

Ford, T. W., & Quiring, S. M. (2019). Comparison of contemporary in situ, model, and satellite remote sensing soil moisture with a focus on drought monitoring. *Water Resources Research*, *55*(2), 1565–1582. https://doi.org/10.1029/2018WR024039

Foreman-Mackey, D., Hogg, D. W., Lang, D., & Goodman, J. (2013). EMCEE: The MCMC hammer. *Publications of the Astronomical Society of the Pacific*, *125*(925), 306–312. https://doi.org/10.1086/670067

Gassenmeier, M., Sens-Schönfelder, C., Delatre, M., & Korn, M. (2014). Monitoring of environmental influences on seismic velocity at the geological storage site for CO_2 in Ketzin (Germany) with ambient seismic noise. *Geophysical Journal International*, *200*(1), 524–533. https://doi.org/10.1093/gji/ggu413

Gaubert-Bastide, T., Garambois, S., Bordes, C., Voisin, C., Oxarango, L., Brito, D., & Roux, P. (2022). High-resolution monitoring of controlled water table variations from dense seismic-noise acquisitions. *Water Resources Research*, *58*(8), e2021WR030680. https://doi.org/10.1029/2021WR030680

Goodman, J., & Weare, J. (2010). Ensemble samplers with affine invariance. *Communications in Applied Mathematics and Computational Science*, *5*(1), 65–80. https://doi.org/10.2140/camcos.2010.5.65

Hassan, D., Burian, S. J., Johnson, R. C., Shin, S., & Barber, M. E. (2023). The Great Salt Lake water level is becoming less resilient to climate change. *Water Resources Management*, *37*(6–7), 2697–2720. https://doi.org/10.1007/s11269-022-03376-x

Heath, D. C., Wald, D. J., Worden, C. B., Thompson, E. M., & Smoczyk, G. M. (2020). A global hybrid VS 30 map with a topographic slope–based default and regional map insets. *Earthquake Spectra*, *36*(3), 1570–1584. https://doi.org/10.1177/8755293020911137

Hobiger, M., Wegler, U., Shiomi, K., & Nakahara, H. (2014). Single-station cross-correlation analysis of ambient seismic noise: Application to stations in the surroundings of the 2008 Iwate-Miyagi Nairiku earthquake. *Geophysical Journal International*, *198*(1), 90–109. https://doi.org/10.1093/gji/ggu115

Hotovec-Ellis, A. J., Shiro, B. R., Shelly, D. R., Anderson, K. R., Haney, M. M., Thelen, W. A., et al. (2022). Earthquake-derived seismic velocity changes during the 2018 Caldera Collapse of Kīlauea Volcano. *Journal of Geophysical Research: Solid Earth*, *127*(2), e2021JB023324. https://doi.org/10.1029/2021JB023324

Hulme, M. (2014). Attributing weather extremes to "climate change" A review. *Progress in Physical Geography*, *38*(4), 499–511. https://doi.org/10.1177/0309133314538644

Hunter, J. D. (2007). Matplotlib: A 2D graphics environment. *Computing in Science & Engineering*, *9*(3), 90–95. https://doi.org/10.1109/mcse.2007.55

Illien, L., Andermann, C., Sens-Schönfelder, C., Cook, K. L., Baidya, K. P., Adhikari, L. B., & Hovius, N. (2021). Subsurface moisture regulates Himalayan groundwater storage and discharge. *AGU Advances*, *2*(2), e2021AV000398. https://doi.org/10.1029/2021AV000398

Kang, J., Walter, F., Halter, T., Paitz, P., & Fichtner, A. (2025). Soil slope monitoring with distributed acoustic sensing under wetting and drying cycles. *EGUsphere*, *2025*, 1–33. https://doi.org/10.5194/egusphere-2025-1725

Khatri, K. B., & Strong, C. (2020). *Climate change, water resources, and potential adaptation strategies in Utah*. Division of Water Resources, Utah Department of Natural.

Landerer, F. W., & Swenson, S. C. (2012). Accuracy of scaled GRACE terrestrial water storage estimates. *Water Resources Research*, *48*(4). https://doi.org/10.1029/2011WR011453

Lecocq, T., Longuevergne, L., Pedersen, H. A., Brenguier, F., & Stammler, K. (2017). Monitoring ground water storage at mesoscale using seismic noise: 30 years of continuous observation and thermo-elastic and hydrological modeling. *Scientific Reports*, *7*(1), 1–16. https://doi.org/10.1038/s41598-017-14468-9

Lesparre, N., Pasquet, S., & Ackerer, P. (2024). Impacts of hydrofacies geometry designed from seismic refraction tomography on estimated hydrogeophysical variables. *Hydrology and Earth System Sciences*, *28*(4), 873–897. https://doi.org/10.5194/hess-28-873-2024

Luu, K. (2021). disba: Numba-accelerated computation of surface wave dispersion [Computer software]. *Zenodo*. https://doi.org/10.5281/zenodo.5775195

Mao, S., Ellsworth, W. L., Zheng, Y., & Beroza, G. C. (2025). Depth-dependent seismic sensing of groundwater recovery from the atmospheric-river storms of 2023. *Science*, *387*(6735), 758–763. https://doi.org/10.1126/science.adr6139

Mao, S., Lecointre, A., van der Hilst, R. D., & Campillo, M. (2022). Space-time monitoring of groundwater fluctuations with passive seismic interferometry. *Nature Communications*, *13*(1), 4643. https://doi.org/10.1038/s41467-022-32194-3

Markovich, K. H., Manning, A. H., Condon, L. E., & McIntosh, J. C. (2019). Mountain-block recharge: A review of current understanding. *Water Resources Research*, *55*(11), 8278–8304. https://doi.org/10.1029/2019wr025676

Mitchell, K. E., Lohmann, D., Houser, P. R., Wood, E. F., Schaake, J. C., Robock, A., et al. (2004). The multi-institution North American Land Data Assimilation System (NLDAS): Utilizing multiple GCIP products and partners in a continental distributed hydrological modeling system. *Journal of Geophysical Research*, *109*(D7). https://doi.org/10.1029/2003JD003823

Namdar Ghanbari, R., & Bravo, H. R. (2011). Evaluation of correlations between precipitation, groundwater fluctuations, and lake level fluctuations using spectral methods (Wisconsin, USA). *Hydrogeology Journal*, *19*(4), 801–810. https://doi.org/10.1007/s10040-011-0718-1

NLDAS project. (2022). In D. M. Mocko (Ed.), *NLDAS Noah Land Surface Model L4 Monthly 0.125 x 0.125-degree V2.0*. NASA/GSFC/HSL, Greenbelt, Maryland, USA, Goddard Earth Sciences Data and Information Services Center (GES DISC). https://doi.org/10.5067/WB224IA3PVOJ

Null, S. E., & Wurtsbaugh, W. A. (2020). Water development, consumptive water uses, and Great Salt Lake. In *Great Salt Lake biology: A terminal Lake in a time of change* (pp. 1–21). https://doi.org/10.1007/978-3-030-40352-2_1

Oakley, D. O., Forsythe, B., Gu, X., Nyblade, A. A., & Brantley, S. L. (2021). Seismic ambient noise analyses reveal changing temperature and water signals to 10s of meters depth in the critical zone. *Journal of Geophysical Research: Earth Surface*, *126*(2), e2020JF005823. https://doi.org/10.1029/2020JF005823

Obermann, A., Planès, T., Hadziioannou, C., & Campillo, M. (2016). Lapse-time-dependent coda-wave depth sensitivity to local velocity perturbations in 3-D heterogeneous elastic media. *Geophysical Journal International*, *207*(1), 59–66. https://doi.org/10.1093/gji/ggw264

Obermann, A., Planès, T., Larose, E., Sens-Schönfelder, C., & Campillo, M. (2013). Depth sensitivity of seismic coda waves to velocity perturbations in an elastic heterogeneous medium. *Geophysical Journal International*, *194*(1), 372–382. https://doi.org/10.1093/gji/ggt043

Okubo, K., Delbridge, B. G., & Denolle, M. A. (2024). Monitoring velocity change over 20 years at Parkfield. *Journal of Geophysical Research: Solid Earth*, *129*(4), e2023JB028084. https://doi.org/10.1029/2023JB028084

Ostrovsky, L. A., & Johnson, P. A. (2001). Dynamic nonlinear elasticity in geomaterials. *La Rivista del Nuovo Cimento*, *24*(7), 1–46. https://doi.org/10.1007/BF03548898

Pacheco, C., & Snieder, R. (2005). Time-lapse travel time change of multiply scattered acoustic waves. *Journal of the Acoustical Society of America*, *118*(3), 1300–1310. https://doi.org/10.1121/1.2000827

Padilla, C., Onda, Y., Iida, T., Takahashi, S., & Uchida, T. (2014). Characterization of the groundwater response to rainfall on a hillslope with fractured bedrock by creep deformation and its implication for the generation of deep-seated landslides on Mt. Wanitsuka, Kyushu Island. *Geomorphology*, *204*, 444–458. https://doi.org/10.1016/j.geomorph.2013.08.024

Perrone, D., & Jasechko, S. (2017). Dry groundwater wells in the western United States. *Environmental Research Letters*, *12*(10), 104002. https://doi.org/10.1088/1748-9326/aa8ac0

Richter, T., Sens-Schönfelder, C., Kind, R., & Asch, G. (2014). Comprehensive observation and modeling of earthquake and temperature-related seismic velocity changes in northern Chile with passive image interferometry. *Journal of Geophysical Research: Solid Earth*, *119*(6), 4747–4765. https://doi.org/10.1002/2013JB010695

Sakaki, T., O'Carroll, D. M., & Illangasekare, T. H. (2010). Direct quantification of dynamic effects in capillary pressure for drainage–wetting cycles. *Vadose Zone Journal*, *9*(2), 424–437. https://doi.org/10.2136/vzj2009.0105

Schmandt, B., Lin, F. C., & Karlstrom, K. E. (2015). Distinct crustal isostasy trends east and west of the Rocky Mountain Front. *Geophysical Research Letters*, *42*(23), 10290–10298. https://doi.org/10.1002/2015GL066593

K. Schwabe, J. Albiac, J. D. Connor, R. M. Hassan, & L. M. González (2013). *Drought in arid and semi-arid regions: A multi-disciplinary and cross-country perspective*. Springer Science & Business Media. https://doi.org/10.1007/978-94-007-6636-5

Schwarz, G. (1978). Estimating the dimension of a model. *Annals of Statistics*, *6*(2), 461–464. https://doi.org/10.1214/aos/1176344136

Seats, K. J., Lawrence, J. F., & Prieto, G. A. (2012). Improved ambient noise correlation functions using Welch's method. *Geophysical Journal International*, *188*(2), 513–523. https://doi.org/10.1111/j.1365-246X.2011.05263.x

Sens-Schönfelder, C., & Eulenfeld, T. (2019). Probing the in situ elastic nonlinearity of rocks with Earth tides and seismic noise. *Physical Review Letters*, *122*(13), 138501. https://doi.org/10.1103/PhysRevLett.122.138501

Sens-Schönfelder, C., & Wegler, U. (2006). Passive image interferometry and seasonal variations of seismic velocities at Merapi Volcano, Indonesia. *Geophysical Research Letters*, *33*(21). https://doi.org/10.1029/2006GL027797

Shen, Z., Yang, Y., Fu, X., Adams, K. H., Biondi, E., & Zhan, Z. (2024). Fiber-optic seismic sensing of vadose zone soil moisture dynamics. *Nature Communications*, *15*(1), 6432. https://doi.org/10.1038/s41467-024-50690-6

Snieder, R., Grêt, A., Douma, H., & Scales, J. (2002). Coda wave interferometry for estimating nonlinear behavior in seismic velocity. *Science*, *295*(5563), 2253–2255. https://doi.org/10.1126/science.1070015

Solazzi, S. G., Lissa, S., Rubino, J. G., & Holliger, K. (2021). Squirt flow in partially saturated cracks: A simple analytical model. *Geophysical Journal International*, *227*(1), 680–692. https://doi.org/10.1093/gji/ggab249

Somers, L. D., & McKenzie, J. M. (2020). A review of groundwater in high mountain environments. *Wiley Interdisciplinary Reviews. Water*, *7*(6), e1475. https://doi.org/10.1002/wat2.1475

Sun, H., Cheng, F., Xia, J., Guan, J., Li, Z., & Ajo-Franklin, J. B. (2025). Unveiling cryosphere dynamics by distributed acoustic sensing and data-driven hydro-thermo coupled simulation. *Geophysical Research Letters*, *52*(2), e2024GL111188. https://doi.org/10.1029/2024GL111188

Takano, T., Nishimura, T., Nakahara, H., Ueda, H., & Fujita, E. (2019). Sensitivity of seismic velocity changes to the tidal strain at different lapse times: Data analyses of a small seismic array at Izu-Oshima Volcano. *Journal of Geophysical Research: Solid Earth*, *124*(3), 3011–3023. https://doi.org/10.1029/2018JB016235

Tangdamrongsub, N., Han, S. C., Yeo, I. Y., Dong, J., Steele-Dunne, S. C., Willgoose, G., & Walker, J. P. (2020). Multivariate data assimilation of GRACE, SMOS, SMAP measurements for improved regional soil moisture and groundwater storage estimates. *Advances in Water Resources*, *135*, 103477. https://doi.org/10.1016/j.advwatres.2019.103477

Tozer, B., Sandwell, D. T., Smith, W. H., Olson, C., Beale, J. R., & Wessel, P. (2019). Global bathymetry and topography at 15 arc sec: SRTM15+. *Earth and Space Science*, *6*(10), 1847–1864. https://doi.org/10.1029/2019EA000658

Tsai, V. C. (2011). A model for seasonal changes in GPS positions and seismic wave speeds due to thermoelastic and hydrologic variations. *Journal of Geophysical Research*, *116*(B4), B04404. https://doi.org/10.1029/2010JB008156

Utah State Water Resource Plan. (2021). Utah department of natural resources. Retrieved from https://water.utah.gov/2021waterplan/

Viens, L., Denolle, M. A., Hirata, N., & Nakagawa, S. (2018). Complex near-surface rheology inferred from the response of greater Tokyo to strong ground motions. *Journal of Geophysical Research: Solid Earth*, *123*(7), 5710–5729. https://doi.org/10.1029/2018JB015697

Vittecoq, B., Burtin, A., & Fortin, J. (2025). Correlating groundwater level fluctuations of a fractured confined aquifer with relative variations in seismic velocity: A way to estimate the groundwater storage. *Geophysical Research Letters*, *52*(7), e2024GL110808. https://doi.org/10.1029/2024GL110808

Voisin, C., Garambois, S., Massey, C., & Brossier, R. (2016). Seismic noise monitoring of the water table in a deep-seated, slow-moving landslide. *Interpretation*, *4*(3), SJ67–SJ76. https://doi.org/10.1190/INT-2016-0010.1

Wada, Y., Van Beek, L. P., Van Kempen, C. M., Reckman, J. W., Vasak, S., & Bierkens, M. F. (2010). Global depletion of groundwater resources. *Geophysical Research Letters*, *37*(20). https://doi.org/10.1029/2010GL044571

Wang, S. Y., Gillies, R. R., & Reichler, T. (2012). Multidecadal drought cycles in the Great Basin recorded by the Great Salt Lake: Modulation from a transition-phase teleconnection. *Journal of Climate*, *25*(5), 1711–1721. https://doi.org/10.1175/2011JCLI4225.1

Weaver, R. L., Hadziioannou, C., Larose, E., & Campillo, M. (2011). On the precision of noise correlation interferometry. *Geophysical Journal International*, *185*(3), 1384–1392. https://doi.org/10.1111/j.1365-246X.2011.05015.x

Weaver, R. L., & Lobkis, O. I. (2004). Diffuse fields in open systems and the emergence of the Green's function (L). *Journal of the Acoustical Society of America*, *116*(5), 2731–2734. https://doi.org/10.1121/1.1810232

Wessel, P., Luis, J. F., Uieda, L. A., Scharroo, R., Wobbe, F., Smith, W. H., & Tian, D. (2019). The generic mapping tools version 6. *Geochemistry, Geophysics, Geosystems*, *20*(11), 5556–5564. https://doi.org/10.1029/2019GC008515

Wu, C., Wu, X., Lu, C., Sun, Q., He, X., Yan, L., & Qin, T. (2022). Characteristics and driving factors of lake level variations by climatic factors and groundwater level. *Journal of Hydrology*, *608*, 127654. https://doi.org/10.1016/j.jhydrol.2022.127654

Xia, Y., Mitchell, K., Ek, M., Cosgrove, B., Sheffield, J., Luo, L., et al. (2012). Continental-scale water and energy flux analysis and validation for North American Land Data Assimilation System project phase 2 (NLDAS-2): 2. Validation of model-simulated streamflow. *Journal of Geophysical Research*, *117*(D3). https://doi.org/10.1029/2011JD016051

Xia, Y., Mitchell, K., Ek, M., Sheffield, J., Cosgrove, B., Wood, E., et al. (2012). Continental-scale water and energy flux analysis and validation for the North American Land Data Assimilation System project phase 2 (NLDAS-2): 1. Intercomparison and application of model products. *Journal of Geophysical Research*, *117*(D3). https://doi.org/10.1029/2011JD016048

Yates, A. S., Savage, M. K., Jolly, A. D., Caudron, C., & Hamling, I. J. (2019). Volcanic, coseismic, and seasonal changes detected at White Island (Whakaari) volcano, New Zealand, using seismic ambient noise. *Geophysical Research Letters*, *46*(1), 99–108. https://doi.org/10.1029/2018GL080580

Yuan, C., Bryan, J., & Denolle, M. (2021). Numerical comparison of time-frequency-and wavelet-domain methods for coda wave interferometry. *Geophysical Journal International*, *226*(2), 828–846. https://doi.org/10.1093/gji/ggab140